The United Nations University

GEOTHERMAL TRAINING PROGRAMME
Orkustofnun, Grensásvegur 9,
IS-108 Reykjavík, Iceland

Reports 2004
Number 18

GEOCHEMICAL INTERPRETATION OF THERMAL WATER AND GAS SAMPLES FROM KRÝSUVÍK, ICELAND AND ALID, ERITREA

Ermias Yohannes Berhane
Ministry of Energy and Mines
Department of Mines, Geological Survey
P.O. Box 272, Asmara,
ERITREA
ermias_yohannes@yahoo.com

ABSTRACT

Krýsuvík, Iceland and Alid, Eritrea are two geothermal fields located within plate tectonic rift zones; an environment characterized by high heat-flow. In this paper, geochemical data from these two systems are reviewed and interpreted. The objective of this study is to explore the potential of geochemical methods to predict the reservoir temperatures and evaluate equilibrium conditions for the two fields.

Eighteen silica and cation geothermometers were used to calculate temperatures for 19 fluid samples from Krýsuvík. Temperatures calculated by various solute geothermometers were generally higher than measured temperatures and the discrepancy between measured and calculated temperatures increased with decreasing temperature. This is indicative of mixing between ground water and geothermal fluids. Mixing was further established by a SiO_2-enthalpy mixing model that predicted two reservoirs for Krýsuvík with temperatures equal to 270ºC and 203°C. The agreement of seven geothermometers was not very good as predicted temperatures commonly varied by about 70ºC for individual samples. However, the discrepancy between the gas geothermometers was more or less constant for different samples, i.e., most of the geothermometers predicted similar differences between the hot and cold samples. The results of the H_2 geothermometer was generally close to the average of other gas geothermometers, ranging between 193 and 270°C with an average value of 238°C in good agreement with measured temperatures and results of solute geothermometers. A map showing isothermal contour lines based on gas geothermometer temperatures of the Krýsuvík area reveals two anomalous semi-linear features, one E-W trending near Krýsuvík, and another NE-SW trending near Trölladyngja.

The Alid water samples are characterized by low pH and high sulphate content, typical of steam heated surface waters. As a result, solute geothermometers do not represent temperatures of the geothermal reservoir. This is reflected by low quartz-geothermometer temperatures (80-224ºC) compared to the gas-thermometer temperatures that range between 163 and 364°C with an average of 272ºC. The results indicate that the geothermal reservoir at Alid is vapour-dominated and surface thermal waters are derived from shallow, steam heated ground water reservoirs.

1. INTRODUCTION

At constructive plate boundaries, new crust is formed by volcanic activity. The new, thin crust is characterized by high heat flow due to the volcanic activity and by extensional tectonics, thus providing the right conditions for high-temperature geothermal activity. The Mid-Atlantic Ridge and the African Rift valley are among the constructive margins in the world that bear numerous sites of geothermal activity. Iceland and Kenya are notable examples of the Mid-Atlantic Ridge and African Rift, respectively. Eritrea, which lies on the northern portion of the African Rift, may have similar prospects of geothermal potential, evidenced from the presence of promising surface manifestations.

This study presents geochemical evaluation of the conditions of mineral equilibria and estimation of subsurface temperatures from geothermal fluids of the wells and hot springs of Krýsuvík geothermal field, Iceland and selected hot springs of Alid geothermal field, Eritrea. Mixing processes that have affected the compositions of the geothermal fluids in the upflow zone before reaching the springs will also be assessed. Geochemical methods provide powerful, efficient and relatively inexpensive tools for assessing reservoir temperature through analysing surface samples. Geochemical exploration is, therefore, very important in the early stages of evaluation of geothermal systems since reservoir temperature is the main factor that determines the potential use of a particular geothermal resource (Arnórsson, 2000).

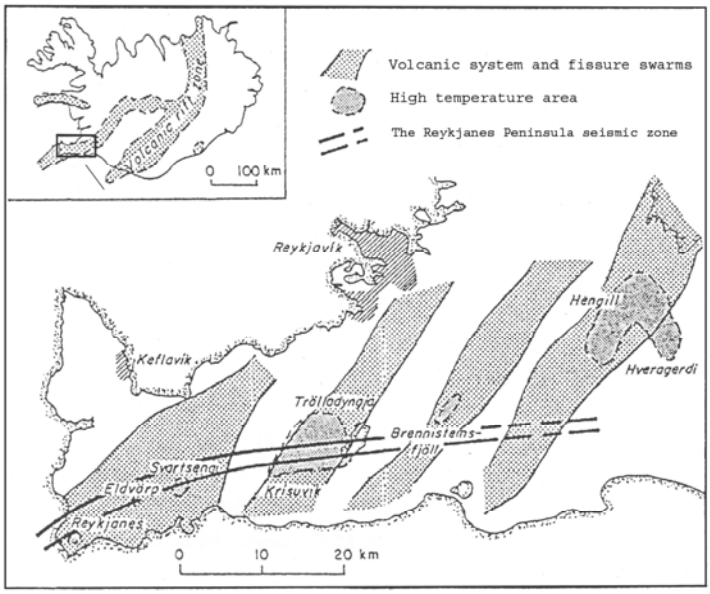

FIGURE 1: Location map of the Krýsuvík area within the volcanic rift zone and high-temperature geothermal areas of the Reykjanes Peninsula

The Reykjanes Peninsula is a neovolcanic segment of the landward extension of the Reykjanes Ridge, where a transform fault shifts the rift zone to the east (Figure 1). It is characterized by high enthalpy flow as a result of the thin crust in this region. Intense volcanic, seismic and high-temperature geothermal activity forms an integral part of the peninsula rift zone. The Krýsuvík area is one of five high-temperature fields on the Reykjanes Peninsula. Other high-temperature areas in Iceland are also located within the active volcanic belts or marginal to them (Arnórsson, 1995).

Owing to the extensive surface manifestations, interest focused on the Krýsuvík geothermal field as early as 1756, when the first hole was drilled. In 1962, three exploratory wells (wells H-1, H-2 and H-3) were drilled, but the results were disappointing. A systematic exploration survey to assess the characteristics of the geothermal reservoir accompanied by drilling did not begin in the area until 1970 (Arnórsson et al., 1975). This research project was comprehensive in that it included detailed geological, geophysical and geochemical assessment and drilling of an additional 4 exploratory wells (wells H-5, H-6, H-7 and H-8). Orkustofnun and Vatnaskil Consulting Engineers conducted an assessment on freshwater and geothermal potential for Lindalax Ltd. (Flóvenz et al., 1986). A feasibility assessment for the Krýsuvík-Trölladyngja area, carried out in 1994, indicated that steam cost estimation was hampered by limited flow rate, thus it was proposed that two wells be drilled in the area (Ármannsson et al., 1994).

Alid is located at the northern part of the East African rift valley close to where the active continental rifting culminates into sea floor spreading in the Red Sea (Figure 2). It runs approximately NNW-SSE

and continues conspicuously to the south, which eventually intercepts the Afar triple junction. This zone has been seismically, tectonically and volcanically active throughout the Late Holocene and Quaternary (Williams et al., 2004). Manifestations of rift succession occur in the form of faults, tensional fissures and volcanic activity. This zone of the East African rift valley is influenced by the presence of the Afar hot spot (Mohr et al., 1978).

FIGURE 2: Location map of Eritrea and the Alid geothermal field

The Alid geothermal field has been recognized as a potential high-enthalpy geothermal resource for several decades due to the evidence of various surface manifestations and the presence of magma within the context of spreading related basaltic volcanism (UNDP, 1973; Beyth, 1994). The first preliminary assessment was carried out by Angelo Marini in 1901 (Marini, 1938). In 1996, a team from the USGS and Eritrean counterparts assessed the geothermal potential of Alid through geological mapping, geochronology and geochemical sampling (Clynne et al., 1996; Lowenstern et al., 1999). This study makes use of geochemical data collected in the 1996 expedition.

2. SAMPLING AND ANALYTICAL METHODS

In this study, gas and water samples from Krýsuvík and Alid collected during 1981-1983 and 1996, respectively, are evaluated. In both cases, water samples were collected in 125, 250, and 500 ml polyethylene bottles. Samples for cation and SiO_2 determinations were acidified with HNO_3. Before acidification, the samples were filtered with a 0.45 µm pore size membrane. Outlet temperature and pH were determined directly in the field. Chemical analyses for the water from Krýsuvík were performed at the Orkustofnun laboratory by the methods summarized in Table 1. Gas chromatography was used to analyse the gas samples from Krýsuvík at the University of Iceland.

Standard procedure as outlined by Giggenbach and Goguel (1989) and Fahlquist and Janik (1992) were used for sample collection in Alid. Steam and gases, including CO_2, H_2, CH_4, H_2S, NH_3, N_2, and Ar, were sampled from fumaroles. A 1-metre long titanium tube was placed on the fumarole covering the cracks and any outlet with mud to minimize air contamination and ensure steam and gas flow. An evacuated Giggenbach bottle, partly filled with NaOH solution was attached to the tube using temperature resistant silicon tubing. Steam and soluble gases condensed within the tube and flowed to the bottle together with bubbles of non-condensable gases. According to the procedures of Fahlquist and Janik (1992), gas chromatography was used for analyses of H_2, N_2, Ar, and CH_4. CO_2 was determined by manometry, H_2S was analyzed by gravimetry and gas sensing electrodes were used to determine the concentration of NH_3. Analyses were conducted at the USGS geothermal laboratory in Menlo Park, California.

TABLE 1: Sample treatment and analytical methods for geothermal water used for Krýsuvík samples

Component	Sample treatment	Analytical method
SiO_2	Raw, diluted	Spectroscopy with ammonium molybdate
Na, K	Filtered acidified	Atomic absorption spectroscopy (flame, Cs added)
Ca, Mg	Filtered acidified	Atomic absorption spectroscopy (flame, La added)
pH, CO_2	Raw, untreated	Titration with HCl using pH-meter
Cl	Filtered, untreated	Ion chromatography
SO_4	Filtered, precipitated	Ion chromatography
F	Filtered, untreated	Selective electrode

3. GEOCHEMICAL METHODS IN GEOTHERMAL EXPLORATION

The application of chemical techniques has become an integral part of any geothermal exploration, especially in the early, pre-drilling stages (Giggenbach, 1991). Geochemical methods are relatively inexpensive and can provide valuable information on the temperature conditions in the geothermal reservoir and the source of geothermal fluid. The use of geochemistry in geothermal exploration has profound importance in inferring subsurface conditions by studying the chemistry of surface manifestations or discharge fluids that carry signature of the geothermal system.

The chemical composition in fluid moving through fractures and pore spaces will be modified spatially and temporally, by chemical interactions with the bed rock and/or by mixing with other fluids. The chemical composition of the parent fluid is either conserved, keeping the original composition, or modified through the flow paths controlled by the flow media. Chemically inert constituents that are conserved and not changed by chemical reactions provide information on the sources of the fluid. Such components are termed tracers. On the other hand, reactive components, such as SiO_2, CO_2, H_2S etc., react with the minerals and other reactive constituents and can contain information about the subsurface condition. Such components are called geoindicators (Arnórsson, 2000). Geothermometers are geoindicators that can be used to estimate subsurface temperatures using the chemical and isotopic composition of hot spring and fumarole discharges.

3.1 General classification and plots

Giggenbach (1991) proposed a SO_4-Cl-HCO_3 ternary diagram for initial classification of geothermal solutions to identify whether the geothermometers are applicable for the given water sample, as most solute geothermometers work only for neutral waters. According to Giggenbach (1991), solute geothermometers can only be applied to what is referred to as “mature waters”, characterized by high Cl and low SO_4 (indicated by a shaded region). This diagram is also helpful in providing an initial indication of mixing relationships. The degree of separation from the Cl towards the HCO_3 is the result of interaction of the CO_2 charged fluids at lower temperatures.

3.2 Geothermometry

Temperature sensitive equilibria between minerals, geothermal solutions, and in some cases a vapour phase can affect the chemical composition of a geothermal fluid, providing the basis for chemical geothermometry. Chemical geothermometers are normally applied to thermal springs, steam vents, and geothermal wells for inferring reservoir temperatures in geothermal exploration and exploitation. The most widely used geothermometers are based on silica concentrations, cation ratios (mainly Na/K), and gas ratios and concentrations in the steam phase. Selected geothermometers of these types are described below.

3.2.1 Silica geothermometers

Temperature-sensitive quartz solubility controls the silica concentration in geothermal fluids in high-temperature geothermal systems. Considerable efforts have been made to measure the quartz solubility and interpret the silica concentrations in thermal springs and geothermal wells. Morey et al. (1962) and Fournier and Rowe (1962) plotted the logarithm of the concentration of dissolved silica versus the reciprocal temperature for quartz and various phases of silica, respectively. They discovered that the data fell along a straight line over the temperature range 20-250°C. Fournier presented the first geothermometer in equation form (Fournier, 1977), and later with his co-workers (Fournier and Potter, 1982) derived a polynomial equation for the quartz geothermometer that estimates temperature up to 330°C. The Fournier and Potter (1982) quartz geothermometer is based on several assumptions, including that the fluid is in equilibrium with quartz in the reservoir, the vapour pressure of pure water fixes the pore fluid pressure in the reservoir, there is no mixing of hot and cold water during upflow, and lastly there is either conductive cooling of the ascending water or adiabatic cooling with steam separation at 100°C (Fournier, 1991). The quartz geothermometer of Fournier and Potter (1982) has been widely used. Later, various silica geothermometers have been developed to assess reservoir temperatures from the silica content of natural water in equilibrium with either quartz or chalcedony. Temperatures predicted by these geothermometers are referred to as quartz- and chalcedony temperatures, respectively (Arnórsson, 2000). Generally speaking, the quartz geothermometer is applied in high-temperature reservoirs, and the chalcedony geothermometer in low-temperature reservoirs.

The SiO_2 geothermometer is normally based on a polynomial function describing experimentally determined silica solubility as a function of temperature (Fournier and Potter, 1982). The basic principle reaction describing silica solubility is:

$$SiO_{2,solid} = SiO_{2,aq}$$

where $SiO_{2,solid}$ is either quartz or chalcedony and $SiO_{2,aq}$ refers to aqueous silica.

At pH levels below ~9, nearly all dissolved silica is present in solution as undissociated silicic acid, H_4SiO_2. At higher pH levels, the silicic acid dissociates to form $H_3SiO_4^-$, thus effectively increasing the solubility of silica in water in equilibrium with quartz. Therefore, very high pH levels can lead to overestimation of the reservoir temperature if aqueous speciation of silica is not considered.

Several geothermometers have been developed as more experimental data has become available (e.g. Gunnarsson and Arnórsson, 2000). Verma and Santayo (1997) have recently developed a new silica geothermometer based on statistical treatment of earlier experimental data. Their new geothermometer is proposed through detecting an outlier and rejecting one sample from the data set of Fournier and Potter (1982). The quartz geothermometer was tested experimentally over the temperature range from 100 to 500°C and pressure of 1000 bars, performed well up to 400°C without any effect of fluid composition (Pope et al., 1987). However, Verma (2000) criticized the use of quartz geothermometers, especially its discrepancy at high temperatures arising from the incoherence between the theoretical and experimental solubility data.

The silica geothermometers equations used to calculate the temperature of a reservoir are as follows:

Quartz, no steam loss:

$$T(°C) = \frac{1309}{5.19 - \log S} - 273.15 \quad (1)$$

Quartz, maximum steam loss at 100°C:

$$T(°C) = \frac{1522}{5.75 - \log S} - 273.15 \quad (2)$$

Quartz:

$$T(°C) = - 42.2 + 0.28831\ S - 3.6686\text{x}10^{-4}\ S^2 + 3.1665\text{x}10^{-7}\ S^3 + 77.034\ \log S \quad (3)$$

Quartz:

$$T(°C) = - 53.5 + 0.11236\ S - 0.5559\text{x}10^{-4}\ S^2 + 0.1772\text{x}10^{-7}\ S^3 + 88.390\ \log S \quad (4)$$

Quartz:

$$T(°C) = - 55.3 + 0.36590\ S - 5.3954\text{x}10^{-4}\ S^2 + 5.5132\text{x}10^{-7}\ S^3 + 74.360\ \log S \quad (5)$$

Quartz:

$$T(°C) = - 66.9 + 0.13780\ S - 4.9727\text{x}10^{-5}\ S^2 + 1.0468\text{x}10^{-8}\ S^3 + 87.841\ \log S \quad (6)$$

Quartz:

$$T(°C) = - 44.119 + 0.24469\ S - 1.7414\text{x}10^{-4}\ S^2 + 79.305\ \log S \quad (7)$$

Quartz:

$$T(°C) = 140.82 + 0.23517\ S \quad (8)$$

Chalcedony:

$$T(°C) = \frac{1032}{4.69 - \log S} - 273.15 \quad (9)$$

Chalcedony:

$$T(°C) = \frac{1112}{4.91 - \log S} - 273.15 \quad (10)$$

where S refers to concentration of SiO_2 in ppm and T is the temperature.

Equations 1 and 2 are from Fournier (1977) for temperatures between 25 and 250°C. Equations 3 and 4 are from Fournier and Potter (1982). Equations 5 and 6 are from Arnórsson (2000). Equations 7 and 8 are from Verma and Santayo (1997) and are applicable for temperatures in the range of 20-210°C and 210-310°C, respectively. Lastly, Equations 9 and 10 represent chalcedony geothermometers from Fournier (1977) and Arnórsson et al. (1983), respectively.

3.2.2 Cation geothermometers

Cation geothermometers are commonly used to estimate reservoir temperatures. Of the cation geothermometers, the Na-K geothermometer is the most widely used geothermometer. The Na-K ratio was initially used to identify the upflow zone of a geothermal system, where the lowest values are observed at the centre of the upflow zone (Ellis and Wilson, 1960). Since then, this method has evolved to increasingly more precise calibration of the temperature dependence of the Na/K ratio, resulting in the calibration of the Na/K geothermometer.

The partitioning of sodium and potassium between aluminosilicates and aqueous solutions is strongly temperature dependent. This is generally interpreted to be a result of equilibrium between Na- and K-feldspars and the aqueous solution, described by the reaction:

$$K^+ + Na\text{-}feldspar = K\text{-}feldspar + Na^+$$

The Na-K geothermometer generally gives consistent results for near neutral pH of geothermal waters that have low calcium content, ($\sqrt{Ca}/Na$) < 1. The Na/K geothermometers are generally in agreement with quartz geothermometers but sometimes they yield rather higher results (Ellis and Mahon, 1977). Solute geothermometers, including those based upon silica solubility and Na/K and K^2/Mg ratios (Fournier, 1985 and Giggenbach, 1988), are ideally applied to chloride springs but considered less reliable when applied to low-chloride springs.

Based on this principle, various Na/K cation geothermometers were developed and applied to geothermal exploration (e.g. Fournier and Truesdell, 1973). Nieva and Nieva (1987) presented a geothermometer based on cation exchange and argued that the geothermometer is able to predict the reservoir temperature, based on the composition of relatively dilute hot-spring waters. Recently, a new Na/K geothermometer was developed purely on an empirical basis and calibrated from field data (Can, 2002). The cation geothermometers considered in this study are listed below, *Na*, *K*, and *Ca* refer to the concentrations of these cations in solution in ppm:

$$T(°C) = \frac{856}{.857 + \log(\frac{Na}{K})} - 273.15 \quad (11)$$

$$T(°C) = \frac{883}{.78 + \log(\frac{Na}{K})} - 273.15 \quad (12)$$

$$T(°C) = \frac{933}{.993 + \log(\frac{Na}{K})} - 273.15 \quad \text{at } 25-250°C \quad (13)$$

$$T(°C) = \frac{1319}{1.699 + \log(\frac{Na}{K})} - 273.15 \quad \text{at } 250-350°C) \quad (14)$$

$$T(°C) = \frac{1217}{1.483 + \log(\frac{Na}{K})} - 273.15 \quad (15)$$

$$T(°C) = \frac{1178}{1.47 + \log(\frac{Na}{K})} - 273.15 \quad (16)$$

$$T(°C) = \frac{1390}{1.75 + \log(\frac{Na}{K})} - 273.15 \quad (17)$$

$$T(°C) = \frac{1052}{1 + e^{(1.714\log(\frac{Na}{K}) + 0.252)}} + 76 \quad (18)$$

$$T(°C) = \frac{1647}{\log\frac{Na}{K} + \beta\left[\log(\frac{\sqrt{Ca}}{Na}) + 2.06\right] + 2.47} - 273.15 \quad (19)$$

where $\beta = 4/3$ for T<100°C; and $\beta = 1/3$ for > 100°C

Equation 11 is from Truesdell and Fournier (1976), Equation 12 is from Tonani (1980) and Equations 13 and 14 are from Arnórsson et al. (1983). Equation 15 is from Fournier, (1979) and Equation 16 is from Nieva and Nieva (1987). Equation 17 is from Giggenbach et al. (1983) and the last Na-K geothermometer in Equation 18 is from Can (2002). Equation 19 shows the Na-K-Ca geothermometer given by Fournier and Truesdell (1973).

The Na, K, Ca, and Mg total contents as well as the Na^2/Mg and Na^2/Ca ratios are mainly controlled by the ionic salinity and are therefore hardly suitable for geoindicators (Chiodini et al., 1991). The experimental work of Pope et al. (1987) showed that the Na-K-Ca geothermometer performed well in 0.1 *M* NaCl solution, but did not work well for experiments using 0.01 *M* $NaHCO_3$. Pope et al. (1987)

concluded that the Na-K-Ca ratio is controlled by alteration reactions, i.e., by base exchange involving clays and mica rather than feldspar equilibria.

3.2.3 The Na-K-Mg ternary system

The Na–K–Mg ternary diagram (Giggenbach, 1988) defines the equilibrium state of waters using the relationship between $Na/1000$, $K/100$ and $\sqrt{Mg}$. This method is based on simultaneous consideration of two temperature sensitive cation ratios or geothermometers, i.e., Na/K and $K/\sqrt{Mg}$. The extent of chemical equilibrium between the fluid and hydrothermal minerals is indicated by the agreement between the two geothermometers. The two cation ratios are defined by equilibrium for the following reactions:

$T_{(Na–K)}$ (1): $$K\text{-}feldspar + Na^+ = Na\text{-}feldspar + K^+$$

$T_{(K–Mg)}$ (2): $$2.8\ K\text{-}feldspar + 1.6\ H_2O + Mg^{2+} = 0.8\ K\text{-}mica + 0.2\ chlorite + 5.4\ silica + 2\ K^+$$

The geothermometer equations used for evaluation of the temperatures in the Na-K-Mg system are:

$$T_{K\text{-}Na} = 1390 / (1.75 - \log (Na/K)) - 273.15$$

$$T_{K\text{-}Mg} = 4410 / (14.0 - \log (K^2/Mg) - 273.15$$

where *Na, K* and *Mg* refer to the concentrations of the respective cations.

Water samples on the upper curve in the Na-K-Mg ternary diagram (see e.g. Figure 11 in Section 4.6) are in full equilibrium conditions; samples below the two curves are in partial equilibrium with respect to Na, K and Mg. The samples below the lower curve are referred to as immature water.

3.2.4 SiO_2 and K^2/Mg equilibrium diagram

Another graphical technique, used to evaluate the aqueous solution equilibrium temperature and a potential cooling process, is based on dissolved silica and the K^2/Mg ratio (Giggenbach et al., 1994). In addition to providing an estimate of subsurface temperature, the log (SiO_2) versus log (K^2/Mg) binary plot can help in defining the cooling processes the solution might have experienced, i.e., adiabatic boiling and conductive cooling. Since both chemical systems respond rapidly to temperature changes, they can provide insights to the ultimate equilibration of the water-rock system (Gherardi et al., 2000).

3.2.5 Gas geothermometers

Geothermometers based on gas equilibria have been developed in the last few decades for application to geothermal systems. The important assumption behind gas geothermometers is that the gas is in equilibrium with the water and the rock. The concentrations and ratios of many gas species are sensitive functions of the reservoir temperature. Thus the gas geochemistry develops to determine the equilibrium of any sets of gas species, assuming that chemical equilibrium does exist among the various species at depth in the reservoir (D'Amore, 1991). However, the validity of the geothermometric relation based on the composition of gas depends on the model of the specific subsystem in question (Tonani, 1973). Nearly all of the gas geothermometers are subject to uncertainties due to buffers of oxygen fugacity (Chiodini and Marini 1998), and H_2 fugacity (Taran et al., 1986), as H_2 is known for rapid response to the re-equilibration process during out-pouring of fumaroles (Giggenbach, 1987). Therefore, in this regard, care should be taken for the respective buffers to determine the formation temperature. Boiling generally increases geothermometer temperatures in the early stages because gas preferentially partitions into the vapour phase where gaseous species partially react (Nehring and D´Amore, 1984).
Various gas geothermometers have been developed, since the first gas geothermometers D'Amore and Panichi (1980) developed were applied. Later, a number of gas geothermometers were developed

using different gas species. The gas geothermometers used in this study are from D'Amore and Panichi (1980) and Arnórsson and Gunnlaugsson (1985). The former gas geothermometer is given by:

$$T(°C) = \frac{24775}{\alpha + \beta + 36.05} - 273$$

where

$$\alpha = 2\log\frac{CH_4}{CO_2} - 6\log\frac{H_2}{CO_2} - 3\log\frac{H_2S}{CO_2},$$

CH_4, CO_2, H_2 and H_2S refer to the concentrations of these gases in volume %;

$$\text{and } \beta = 7 \log P_{CO_2}.$$

if $CO_2 < 75\%$ then $P_{CO_2} = 0.1$ atm,
if $CO_2 > 75\%$ then $P_{CO_2} = 1$, and
if $CO_2 > 75\%$ and $H_2S > 2\ H_2$ then $P_{CO_2} = 10$ atm.

The gas geothermometers from Arnórsson and Gunnlaugsson are summarized in Table 2, below.

TABLE 2. Temperature functions of gas geothermometers (Arnórsson and Gunnlaugsson, 1985)

Geothermometer	Temperature function[1]	Applicable range
CO_2	-44.1+269.25Q-76.88Q^2+9.52Q^3	All waters
H_2S	246.7+44.81Q	Valid for all waters above 300°C and waters in the range 200-300°C if chloride >500 ppm
H_2	277.2+20.99Q	
CO_2/H_2	341.7-28.57Q	
H_2S/H_2	304.1-39.48Q	
H_2	212.2+38.59Q	Valid for all waters below 200°C and waters in the range 200-300°C if chloride <500 ppm
H_2S	173.2+65.04Q	
CO_2/H_2	311.7-66.72Q	

[1] Q refers to the logarithm of the respective gas concentration or ratio in moles per kg of steam

Giggenbach (1991) proposed an equilibrium ternary diagram based on a combination of two gas ratios, i.e., log (X_{CO_2}/X_{Ar}) and log (X_{H_2}/X_{Ar}), with X refering to mol fraction, which attain equilibrium at different rates. This may provide a method for assessing the state of equilibrium attainment.

3.3 Mineral saturation

Evaluation of chemical equilibria between minerals and aqueous solutions in natural systems requires determination of the activities of aqueous species and knowledge of the solubilities of the minerals present in the bedrock. Assumption of specific mineral-solution equilibria is necessary to use in applying geochemistry to obtain an understanding of various physical features of a geothermal system.

In this study, the calculation of ion activities and saturation indices of minerals with respect to the calculated water composition was performed using the SOLVEQ program (Reed and Spycher, 2001).

Reed and Spycher (1984) have proposed that the best estimate of reservoir temperature can be attained by simultaneously considering the state equilibrium between specific water and many hydrothermal minerals as a function of temperature. The saturation index of several minerals is computed as a function of temperature and if the saturation indices of the minerals converge to zero (saturation) at a specific temperature, that temperature is taken to represent the reservoir temperature. However, it is to be noted that care should be taken in interpreting the results of multi-mineral/solute equilibria as the results depend on both the thermodynamic data base used for mineral solubilities and the activities of end-member minerals in solid solutions (Tole et al., 1993).

Using the results of the aqueous speciation calculations, the saturation indices (SI) of minerals in aqueous solutions at different temperatures were computed as:

$$SI = \log\frac{Q}{K} = \log Q - \log K \,,$$

where Q is the calculated ion activity product (IAP) and K is the equilibrium constant.

The SI value for each mineral is a measure of the saturation state of the water phase with respect to the mineral phase. Values of SI greater than, equal to, and less than zero represent, supersaturation, equilibrium and undersaturation, respectively, for the mineral phase with respect to the aqueous solution.

Equilibrium constants for mineral dissolution often vary strongly with temperature. Therefore, if the SI's with respect to several minerals converge to zero at a particular temperature, that temperature is taken to be the reservoir temperature.

SOLVEQ is a program used to compute multicomponent homogeneous chemical equilibria for aqueous solutions (Reed, 1982). It computes the activities of all aqueous species, the saturation index of solids, the fugacities of gases at a given temperature, and total composition of gases by solving a system of mass-balance and mass-action equations by the Newton-Raphson numerical technique (Reed, 1982). It also calculates partial heterogeneous equilibrium where equilibration of certain water with a given mineral or gas fugacities can be forced. This ability allows fixing the total concentration of a specified component species. An unknown concentration of aluminium in a given water sample can be computed by forcing equilibrium with kaolinite. This capability, combined with the ability to calculate pH at high temperature from given low T-pH measurements (Pang and Reed, 1998), is also useful in processing hydrothermal geothermometry and other studies of geothermal waters.

3.4 Mixing models

Before emerging to surface via hot springs and fumaroles, geothermal fluids may be affected by various processes. They may cool on the way by conduction, boiling or mixing with shallow cold water or by way of combination of these three processes (Arnórsson, 1985). Cooling is common at various levels both in the natural or exploitation state. In the deeper level, the density difference between the hot and cold water imparts cooler water to encroach into the hot aquifer (Truesdell, 1991). During exploitation, the pressure differences between the hot and cold water increases, thus allows mixing. Cooling and dilution are the effects of mixing. Natural geothermal fluids in hot springs or fumaroles are usually made up of components from two or more sources that cannot be sampled directly. Thus, in order to evaluate a geothermal system by mixing models, the chemical compositions of the individual components have to be identified (Noda and Shimada, 1993).
The three mixing models that are most commonly used to unravel mixing processes in a geothermal system are:

- The chloride-enthalpy mixing model;
- The silica-enthalpy mixing model; and
- The silica-carbonate mixing model

In addition, binary plots of chemical constituents, such as the linear pattern of binary plot of chloride versus boron or $\delta^{18}O$-values are taken to be convincing evidence for mixing (Arnórsson, 1991).

Recognition of mixing based only on the chemical composition of one sample is not compelling. Thus, a considerable amount of samples from groups of springs is needed to establish the nature of potential mixing of hot water and cold water in the upflow zone.

4. THE KRÝSUVÍK GEOTHERMAL FIELD, SW ICELAND

4.1 Geological setting

The Krýsuvík geothermal field is located at one of the five volcanic systems of the Reykjanes Peninsula (Figure 1). Four high-temperature areas occur on the Reykjanes Peninsula, all lying on the plate boundary accompanied by fault swarms, oriented in en-echelon array at an average angle of ~40°N (Klein et al., 1973). The volcanic rocks of the Reykjanes Peninsula are exclusively basaltic in composition, lacking evolved compositions that commonly occur in central volcanos of other parts of Iceland. (e.g. Jakobsson, 1979; Saemundsson, 1979). Subglacial hyaloclastites intercalated with sub-aerial lava flows and pyroclastic facies dominate the stratigraphy of the area (Figure 3). The presence of hyaloclastites and lavas is a result of periodical presence of glaciations. These successions of Upper Pleistocene interglacial basalts and hyaloclastites and Holocene lavas make up the succession of the Krýsuvík surface rocks. The hyaloclastite ridges of Sveifluháls and Vesturháls formed during sub-glacial fissure eruptions of the last glaciation period (Jónsson, 1978).

Sub-aerial volcanic products and landscape features like explosion craters or lava flows manifest the volcanic activity during the ice-free periods in the Krýsuvík area (Vargas, 1992). Three postglacial lavas overlie the largest interglacial lava outcrop in the southern part of the area. The postglacial lavas flowed mainly in Krýsuvík valley in between the ridges. The northernmost lava flow reached the water of lake Kleifarvatn. Tephrochrono-logical studies indicate that the age of these postglacial volcanics is some 2000 years. In addition to the lava flows, pyroclastic lavas and explosion debris are common. Unlike the surrounding areas, several explosion craters (maars) occur in the Krýsuvík area (Figure 3).

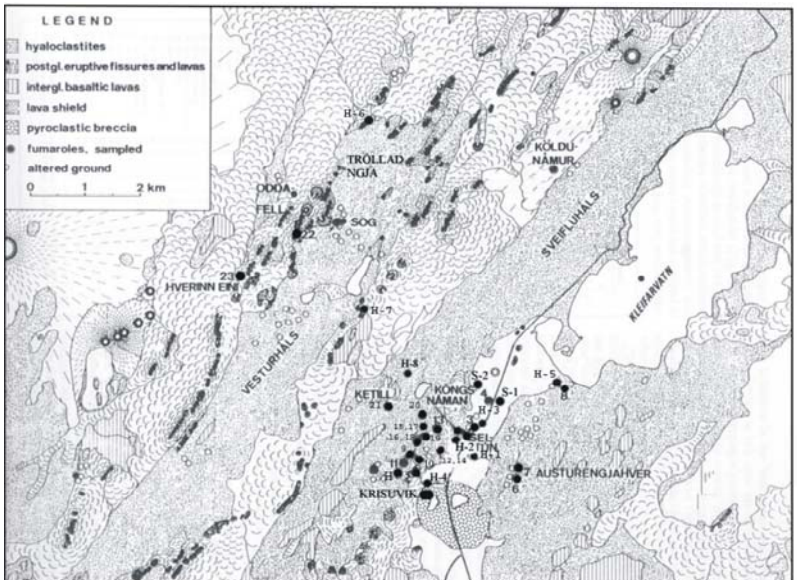

FIGURE 3: Geological and sample location map of Krýsuvík area (from Arnórsson, 1987)

In addition to the widespread volcanics, sedimentary formations of glacial, aeolian, lacustrine, and fluvial origin occur in the Krýsuvík valley. The glacial sediments, or tillites are often deposited on the slopes of the mountains

and lower ground. Although typical alluvium of fluviatile origin was not observed, clay rich alluvium is common in the valley between Kleifarvatn and Graenavatn. Lacustrine deposits are confined to a small closed basin such as filling up explosion craters. Aeolian sediments in the area consist of thin, fine-grained, laminated sandy soils in a thin layer, continuous in the plain but as remnants among the hills (Vargas, 1992).

The Krýsuvík-Trölladyngja fissure swarms are among the largest en-echelon structures in the Reykjanes Peninsula. The continuous tectonic activity of the area is manifested by greater density of fractures in the Upper Pleistocene interglacial lava formations than in younger lavas. The ridges are parallel to the fissure swarms illustrating the connection between tectonics and volcanic activity. Subareal crater rows have also the same orientation as the fissure swarms. The fissure swarms of the Reykjanes Peninsula are commonly interpreted as rift zones interconnected by transform faults. The permeability of the hyaloclastite ridges of Vesturháls and Sveifluháls and a fault running through Austurengjahver hot spring (Figure 3) and associated fissure swarms play an important role in characterizing the geothermal flow and storage at depth.

4.2 Resistivity survey of Krýsuvík

The relative water table position, water salinity, bedrock alteration, and underground temperature influence the bedrock resistivity in Krýsuvík (Georgsson, 1987). Kebede (2001) and Ha Ngoc Hung (1997) have compiled Schlumberger surveys into contoured resistivity maps at various depth levels. The resistivity maps for 150 m a.s.l. and at sea level are shown in Figure 4. The wide spread low-resistivity areas in the uppermost 500 m correspond to geothermal activity. Similar results showing low-resistivity area at 300 m a.s.l. in the Trölladyngja-Krýsuvík area were interpreted earlier to represent upflow zones (Georgsson, 1987). The major zone has a trend similar to the main volcanic fissure swarms with a N45°E orientation. This might correspond to the hyaloclastite lithological unit. The isoresistivity map in Figure 4a shows that a strong NE-SW elongated resistivity low is located along the western roots of Trölladyngja and another more irregular low-resistivity anomaly is seen in the Krýsuvík area. High-resistivity values are predominant at the surface in Postglacial lava fields

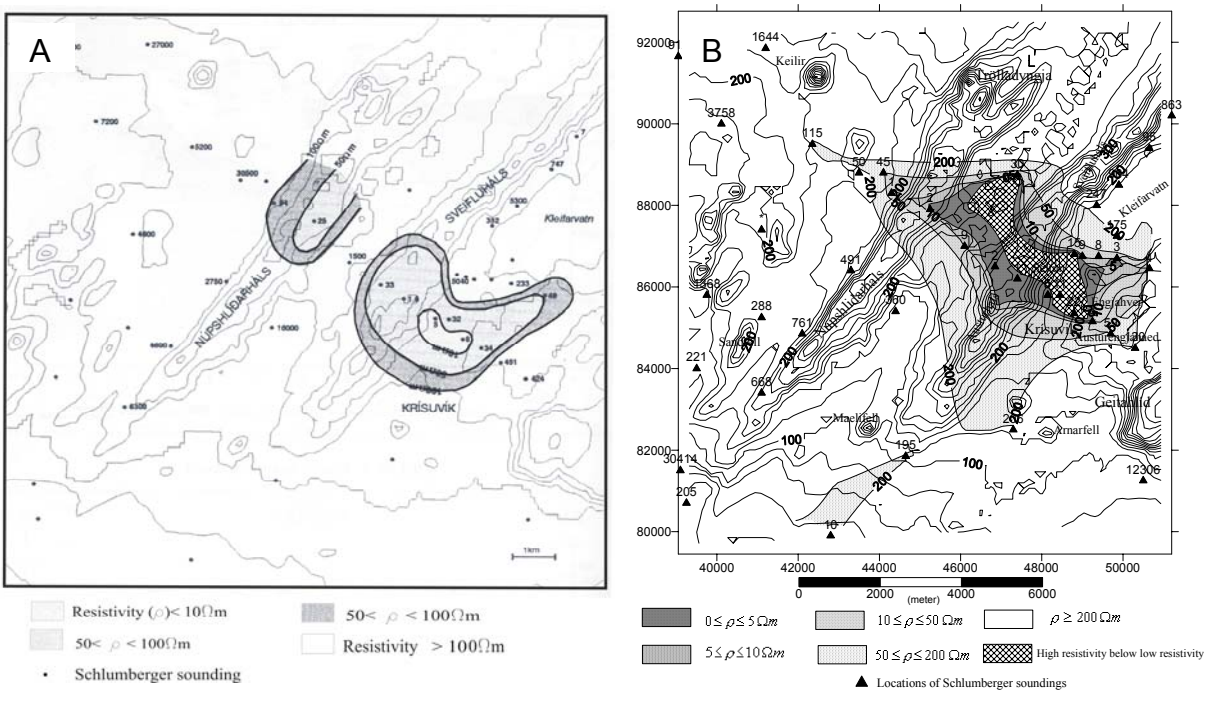

FIGURE 4: Isoresistivity maps of the Krýsuvík area at a) 150 m a.s.l. (Ha Ngoc Hang, 1997) and b) at sea level (Kebede, 2000)

except in areas affected by surface acid leaching. A high-resistivity body underlies the low-resistivity anomaly (Figure 4b). This is a result of a transition in dominant alteration minerals, from smectite to chlorite and epidote (Flóvenz et al., 1986). This mineralogical transition occurs at about 240°C and it, thus, reflects higher temperatures. A possible alternative explanation is that this change in resistivity is a result of a temperature reversal.

4.3 Geothermal manifestations

Geothermal manifestations in the Krýsuvík field include fumaroles, hot altered ground, and steam heated acidic pools (Arnórsson, 1987). The geothermal activity is scattered over a large area within the fissure swarms (Flóvenz et al., 1986). On the basis of surface manifestation, Arnórsson (1987) subdivided the area into two: the Sveifluháls and the Vesturháls areas. Steam-heated pools are confined to the Sveifluháls area. Except in Sog, acid alteration is limited in Vesturháls. The tectonic control of the upflow of the geothermal fluid is manifested by the common occurrence of fumaroles and hot grounds within faults and fissures.

4.4 Sub-surface geology and hydrothermal alteration

Orkustofnun and Vatnaskil Consulting Engineers performed an evaluation of the data from the existing wells in the Krýsuvík area (Flóvenz et al., 1986). In this area, eight shallow to deep exploratory wells have been drilled. All the wells evaluated in this study were drilled in 1970 except for H-3 which was drilled in 1962. The depths of wells H-3, H-5, H-6, H-7 and H-8 are 329, 816, 843, 931, and 930 m, respectively. A temperature reversal at an average depth of 500 meters is observed in most of the drill holes. The geology of the wells is consistent with the stratigraphic succession shown on the geological map in Figure 3. A summary of the borehole logging of well H-6 is shown in Figure 5 and described below.

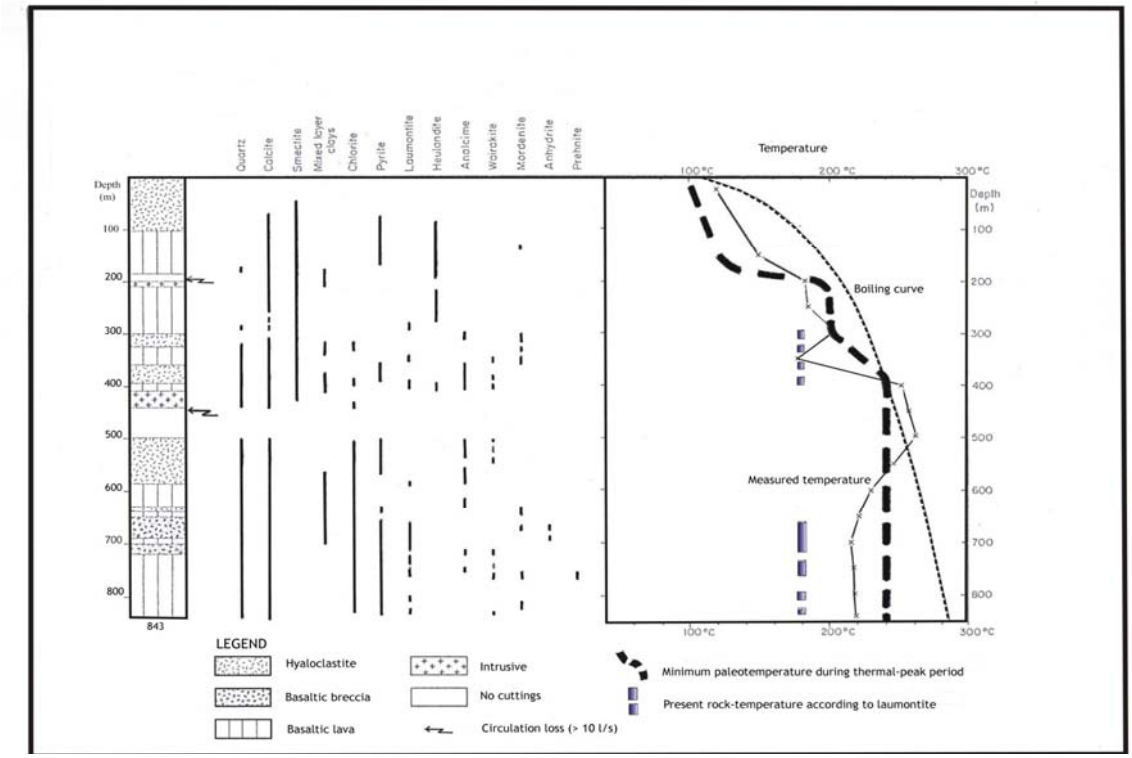

FIGURE 5: Simplified stratigraphic profile of well H-6 showing lithostratigraphic units, distribution of alteration minerals, and temperature-depth profile (Flóvenz et al., 1986)

Hyaloclastites and basaltic lavas interlayered with intrusions make up the stratigraphic profile of the well. Basaltic lava is at the bottom of the well (843 m) and extends up to 600 m with an intercalation of basaltic breccia. A hyaloclastite unit overlies the basaltic lava unit and continues up to a depth of 500 m. The hyaloclastites are pervasively altered between 500 and 585 m depth. Owing to lack of rock cuttings, no information is available on the stratigraphic interval between 440 to 500 m depth. Basaltic lava is the major rock unit, with only few layers of hyaloclastites in the stratigraphic column from 200 to about 400 m. Hyaloclastite occurs in the uppermost 100 m of the succession.

The most important observation of the stratigraphic logging is the presence of two coarse-grained, presumably dolerite, dykes at about 200 m and at 410-442 m depths. These dykes may have acted as feeders to some of the lavas occurring at surface. This is supported by the close resemblance of the dykes to some of the only postglacial rocks in the region. High circulation losses or aquifer sites are recorded by the dykes. Although the upper part of the dykes coincides with the bottom of the 5″ casing, the position of the lower dyke corresponds to the highest measured temperature. This suggests that the dyke is the centre of an upflow zone fed by a hotter reservoir at depth.

Lithological logging of well 6 also reveals important information on the occurrence and distribution of alteration minerals. The trace of the paleotemperature profile is drawn based on information from the mineral formation temperatures (Figure 5). Calcite deposition occurs between 200 and 300 m interpreted as a cap rock. Calcite superimposes heulandite, but information on the paleotemperature is unclear. The assemblage of quartz, wairakite and clay minerals at 300-350 m suggest the paleotemperature was more than 200°C at that depth interval and increased to 240°C close to 400 m, where chlorite becomes the dominant clay mineral. Detailed information on the evolution of mineralogical alteration at the bottom portion is inadequate due to the extremely fine-grained rock cuttings. Laumontite is sparse at 300-400 m and appears thermally altered close to 400 m depth. The appearance of laumontite at this depth may imply that some cooling has already taken place within the upper part of the reservoir (Figure 5). Laumontite is absent at 400-650 m depth, but is quite abundant at 650-750 m depth. The freshness and abundance of this mineral below 650 m depth implies that the present rock temperature may be considerably lower than that of the measured temperature (220°C) profile. The discrepancy could be a result of fluid movement between aquifers of different levels within the well. If this is true, the potential high-temperature zone is more restricted than anticipated from the measured temperature profile.

The overall data on the hydrothermal alteration indicates a rather localized occurrence of high-temperature fluids (with temperatures higher than 250°C) at depths between 400 and 500 m. Two hypotheses are developed to explain the inverse temperature profile; the first is a mushroom shaped model where a hot temperature reservoir flows on top of cold water. The other assumes a gradual cooling from top and bottom of the reservoir.

4.5 Chemical composition of the Krýsuvík samples

The geochemical data of Krýsuvík are gathered from various sources; well fluid samples and two spring samples are from Arnórsson et al. (1975), whereas the gas samples are from Arnórsson (1987) and Ólafsson, (1991). The analytical data for the water samples include concentrations of SiO_2, Na^+, K^+, Ca^{2+}, Mg^{2+}, CO_2 (total), SO_4, F, B, and total dissolved solids (TDS) from the wells at different sampling levels (Table 3). Analysis of gas samples from Krýsuvík fumaroles are listed in Table 4.

Binary plots

Binary plots of cations, SO_4, TDS and silica versus chloride are plotted on Figure 6. The TDS values, ranging from 208 to 2605 ppm, are directly proportional to the chloride content. A similar linear pattern is also displayed for Na and SiO_2, although the relationship between SiO_2 and Cl is somewhat dispersed at higher chloride content. The concentrations of Na, SiO_2 and Cl, as well as TDS, increase

TABLE 3: Chemical composition of Krýsuvík water samples (Arnórsson et al., 1975), in ppm (SD is sampling depth, TS is temperature at sampling depth)

Location	SiO_2	B	Na^+	K^+	Ca^{++}	Mg^{++}	CO_2x	SO_4^{2-}	H_2S	Cl^-	F^-	TDS	SD	TS
S 1	133	-	42	3.5	32.4	32.5	14.5	29	<.1	42.3	0.1	552		
S 2	77	-	34.3	2.8	52.4	21.2	14.1	69.5	<.1	21.2	0.1	426		
H-3 300	154	-	148	12.8	19.1	1.3	310	31.9	<.1	70.4	0.15	654	300	115
H-5 200	222	1.25	206	21.5	9.4	0.24	96	157	3.3	102	0.34	856	200	173
H-5 350	226	1.23	205	12.9	9.1	0.24	55	175.3	0.3	122	-	850	350	154
H-5 470	220	1.18	210	13.8	10.6	2.22	63	178.2	4.4	118	0.45	861	470	151
H-5 650	210	1.15	200	12.9	10	0.23	72	141.6	0.2	151.5	-	822	650	151
H-5 800	164	0.59	233	16.7	16.5	0.51	63	324.7	1.3	52	0.6	896	800	151
H-6 200	205	0.65	680	40.4	90.8	0.5	55.7	103.1	<.1	1234	0.2	2563	200	183
H-6 500	514	0.79	700	119	42.4	0.38	62.2	49.6	6.6	1094	0.5	2605	500	258
H-7 325	50	-	30.6	1.7	18.4	10.4	110	7.9	<.1	16.1	0.2	208	325	30
H-7 475	178	0.14	160	8.2	15.3	1.4	120	75.1	<.1	163.2	0.4	692	475	139
H-8 240	210	0.24	140	8.3	5.5	0.3	66.9	90	<.1	96.8	0.7	600	240	129
H-8 450	332	0.52	227	21.5	11.5	0.13	121	240	<.1	246.4	0.7	1000	450	192
H-8 700	332	0.5	230	20.8	12.5	0.14	117.5	106.3	<.1	245.6	0.8	1000	700	184
H-8 920	298	0.53	226	21.3	17	0.23	121	104	<.1	244	0.8	1030	920	170
H-14	490	1.77	465	57.2	10.4	0.04	49.8	92.4	<.1	759	0.3	1876	-	-
H-6 800	304	0.39	596	64	0	0.44	59.5	40.1	1.7	914	0.3	2020	800	218
H-3 200	142	-	-	10.8	24.6	1.4	316	31.3	<.1	34.4	0.1	610	200	105

TABLE 4: Chemical data of the gas samples of the Krýsuvík area, in mmoles gas/kg steam (all samples are from Arnórsson (1987) except those with asterisk that come from Ólafsson (1991))

Sample	CO_2	H_2S	H_2	O_2	CH_4	N_2	Ar
1	302	41.33	11.02	0.16	0.115	3.8	0.104
2	271.9	39	7.7	0.15	0.088	4.26	0.104
3	306	42.6	16.28	0.04	0.153	2.42	0.092
4	253	32.78	16.36	0.04	0.156	1.65	0.093
5	279.4	15.32	0.38	0.03	0.027	1.34	0.063
6	205.7	20.49	9.06	0.06	0.1	3.31	0.15
7	258	28.5	14.71	0	0.286	74.84	1.29
8	279.2	12.92	30.91	0	0.939	9.8	0.197
9	245.6	16.85	9.24	0.1	0.044	1.49	0.052
10	258	15.43	8.82	0.13	0.052	1.76	0.044
11	278.9	17.72	6.76	0.05	0.029	1.61	0.06
12	282.9	16.18	7.12	0.04	0.059	5.42	0.144
13	258.4	16.08	0.78	0.1	0.072	4.18	0.12
14	272.5	23.3	7.09	0.07	0.067	2.5	0.069
15	268.8	19.63	6.56	0.02	0.053	4.42	0.118
16	276	14.64	7.52	0.09	0.222	7.61	0.263
17	286.5	19.15	4.78	0.02	0.049	1.79	0.091
18	317.3	7.74	0.6	0.94	0.098	11.54	0.327
19	241.3	19.48	4.5	0.07	0.025	1.79	0.069
20	429.2	13.72	3.36	0.07	0.39	11.2	0.326
21	111	2.58	0.32	0.08	0.034	2.46	0.052
22	202.8	2.18	0.46	0.01	0.333	8.52	0.378
Seltún (S)*	237.2	41.7	10.5		0.1	1.2	
Hveradalur (H)*	185.9	24.1	4.7		0.06	0.9	
23	965.7	82.51	8.71	46.95		336.5	5.81

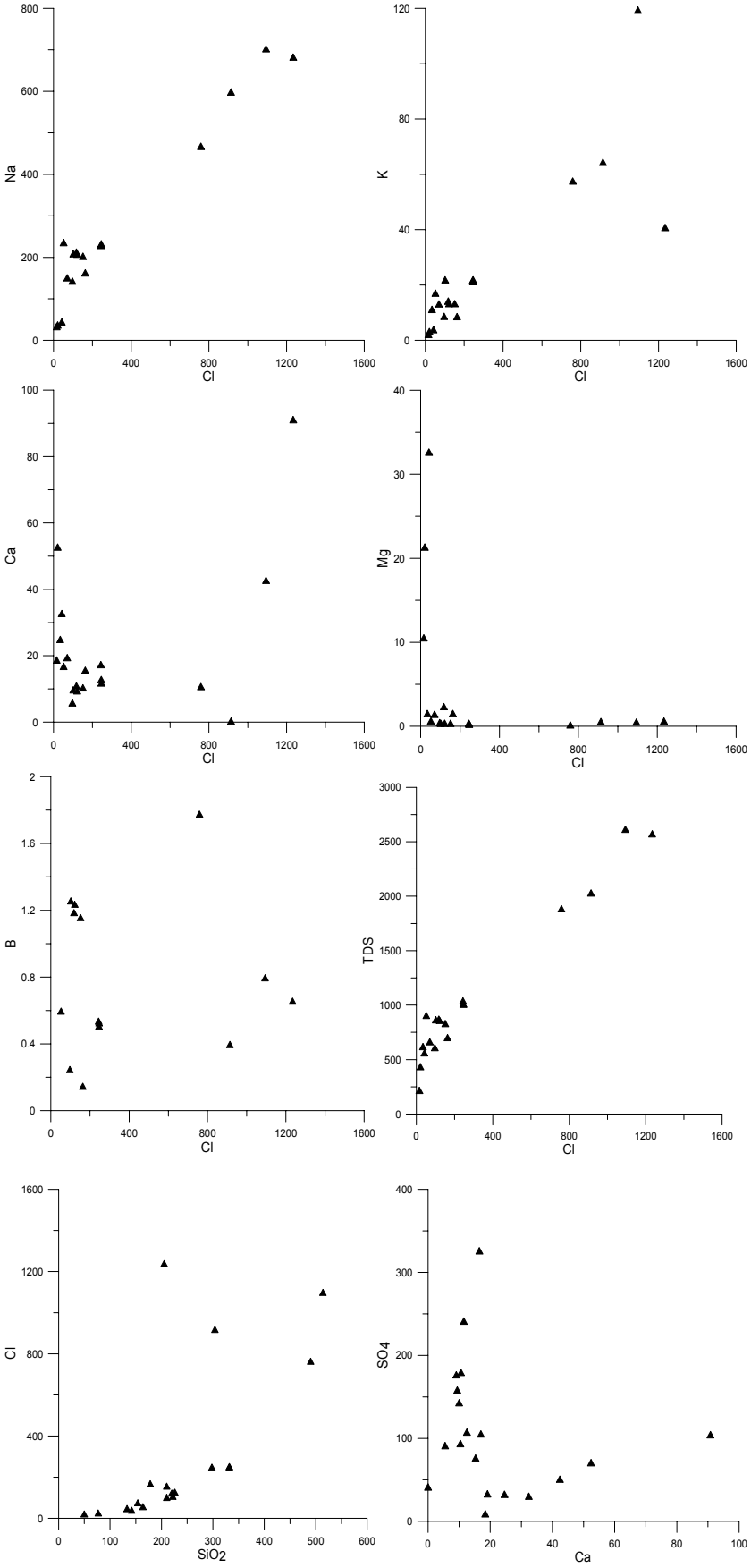

FIGURE 6: Binary plots of Cl vs. cations, B and TDS, SiO_2 vs. Cl and Ca vs. SO_4 for Krýsuvík water samples; units are in ppm

with increasing temperature. No direct relation-ship is observed between boron and chloride indicative of seawater mixing. High magnesium concentrations tend to coincide with low chloride content, although this relationship is not quite clear.

Cl-SO_4-HCO_3 diagram

All the water samples from the Krýsuvík wells lie outside the "mature water" field in Figure 7 with the exception of three samples from well H-6. The majority of the samples are systematically distributed in a nearly linear array between the sulphate and chloride corners. Samples from well H-3 and sample H-7-325 plot close to the HCO_3 corner, which may indicate mixing with cold water.

N_2-CO_2-Ar diagram

The N_2/Ar ratio in free gas from fumaroles varies between 40 and 80 if these gases are solely of atmospheric origin depending on the spring temperature, i.e., springs with higher discharge temperatures have lower N_2/Ar ratios (Mariner et al., 2003). The N_2/Ar values of the Krýsuvík gas samples range from 20 to 58 (Figure 8). It appears most likely that the contribution of air-saturated water is high. Additional argon intro-duction is inferred relative to nitrogen as the samples are shifted towards the argon corner.

4.6 Geothermometry of Krýsuvík wells and springs

All the geothermometers discussed in the previous section were applied to the water and gas samples from the Krýsuvík area that are listed in Tables 3 and 4.

Silica geothermometers

Silica geothermometers generally yield higher temperature values than measured in the drill holes (Table 5). However, for the wells with the highest measured temperatures, the calculated temperature is only slightly higher than the measured one, whereas this difference is bigger for samples at lower temperatures (Figure 9). Samples from well H-5 have measured values only slightly lower than the quartz geothermometer gives, in particular the sample taken at the shallowest depth (200 m) which has only 5°C difference. On the other hand, sample H-5 at 800 m has a calculated value below the upper level samples (similar measured temperature value, 151°C with the adjacent upper levels), despite being taken from the deepest part of the well at 800 m. The three samples of well H-6 exhibit an interesting pattern. The geothermometers predict similar temperatures to the measured ones and temperature increases consistently in all the samples. At the highest measured temperature (258°C of H-8 500) all the calculated temperatures are lower than the measured values, except for Arnórsson's (2000) Equation 4. The calculated temperatures using Fournier (1977) Equation 2, Arnórsson (2000) Equation 5, and Fournier and Potter (1982) correspond well with the measured values, between 180 and 200°C. The calculated temperatures of well H-7 although low have broad disparity with the measured temperature, particularly for samples with the lowest temperature.

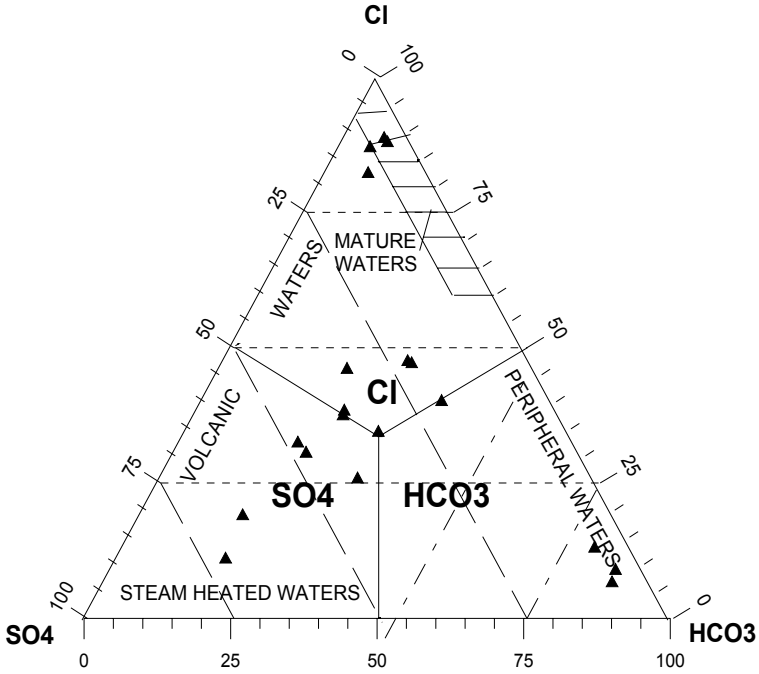

FIGURE 7: Cl-SO_4-HCO_3 classification diagram of Giggenbach (1991) for the Krýsuvík water samples

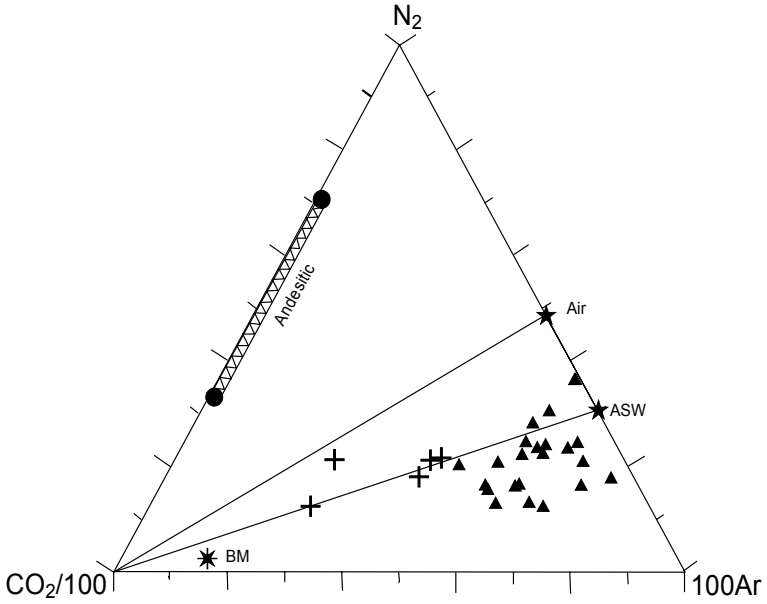

FIGURE 8: N_2-CO_2-Ar diagram for the Krýsuvík gas samples; solid triangles are Krýsuvík gas samples and crosses are Alid gas samples (Lowenstern et al., 1999) for comparison (BM denotes basaltic mantle and ASW is air saturated water)

In general, the lowest temperatures are predicted by the chalcedony geothermometer. Equation 2 (Fournier, 1977) gives agreeable value with measured temperature ranging from 150 to 185°C and

values based on Verma and Santayo (2000) and Equation 4 of Arnórsson (2000) agree well with measured temperatures above 195°C. Equation 3 in Fournier and Potter (1982) can be taken as an average value as it matches with the overall measured temperature values.

TABLE 5: Results of silica geothermometers for Krýsuvík water samples

Sample	TM[1]	F[2]	F[3]	FP[4]	A[5]	A[6]	VS[7]	Average	F[8]	A[9]
S1		154	147	148	143	137	154	146	129	126
S2		123	121	118	110	109	123	116	95	95
H-3 200	105	158	150	152	147	141	158	150	134	130
H-3 300	115	163	154	157	153	145	163	154	139	135
H-5 200	173	187	174	182	180	167	188	178	167	161
H-5 350	154	188	175	183	181	169	189	179	169	162
H-5 470	151	187	174	181	179	167	187	177	166	160
H-5 650	151	183	171	178	176	164	184	174	163	157
H-5 800	151	167	157	161	157	149	167	158	144	139
H-6 200	183	182	170	176	174	162	182	173	161	155
H-6 500	258	255	228	254	267	230	262	247	248	233
H-6 800	218	210	193	205	206	189	211	201	194	185
H-7 325	30	102	103	98	88	89	102	96	72	73
H-7 475	139	172	162	167	163	154	172	164	150	145
H-8 240	129	183	171	178	176	164	184	174	163	157
H-8 450	192	217	198	212	214	195	218	207	203	192
H-8 700	184	217	198	212	214	195	218	207	203	192
H-8 920	170	209	191	204	204	187	210	199	193	183
H-14		250	224	248	259	226	254	242	243	228

[1] Measured temperature;
[2,3] Fournier (1977) Equations 1 and Equation 2, respectively;
[4] Fournier and Potter (1982).
[5,6] Arnórsson (2000) Equation 4 and Equation 5, respectively;
[7] Verma and Santayo (1997);
[8] Chalcedony (Fournier, 1977);
[9] Calcedony (Arnórsson et al., 1983).

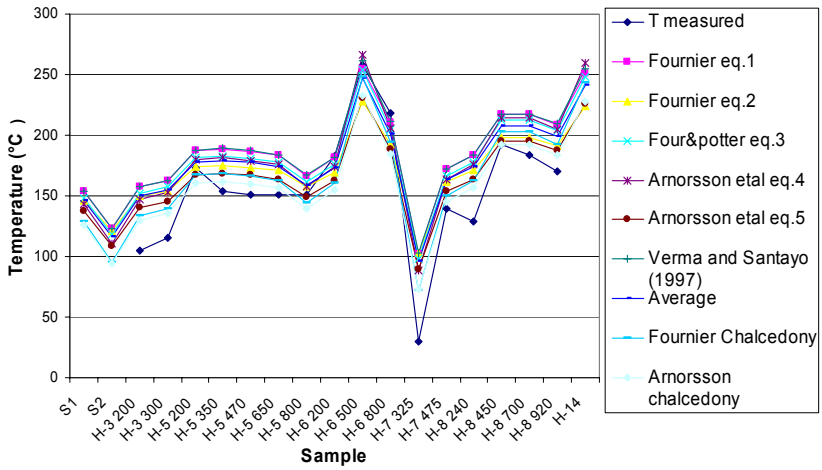

FIGURE 9: Silica geothermometers dispersion pattern of Krýsuvík water samples

Cation geothermometers

Despite that the calculated temperature values of the Na-K geothermometers are generally claimed to be higher than the respective values of quartz geothermometers, the opposite was found to be true for the Krýsuvík water samples (Table 6). The Na/K temperatures agreed more closely with the measured temperature, compared to the silica geothermometers. The cation geothermometers in Equation 12 (Tonani, 1980), Equation 13 (Arnórsson et al., 1983) and Equation 11 (Truesdell; 1976) give reasonable results, except for the samples from H-7 at 325 m, H-6 at 800 m and H-5 at 200 m. The calculated values of almost all of the samples using Fournier (1983), Verma (2000), Can (2002) and Giggenbach et al. (1983) and the Na-K-Ca geothermometer of Fournier and Truesdell (1973) are higher than the measured values. The extremely

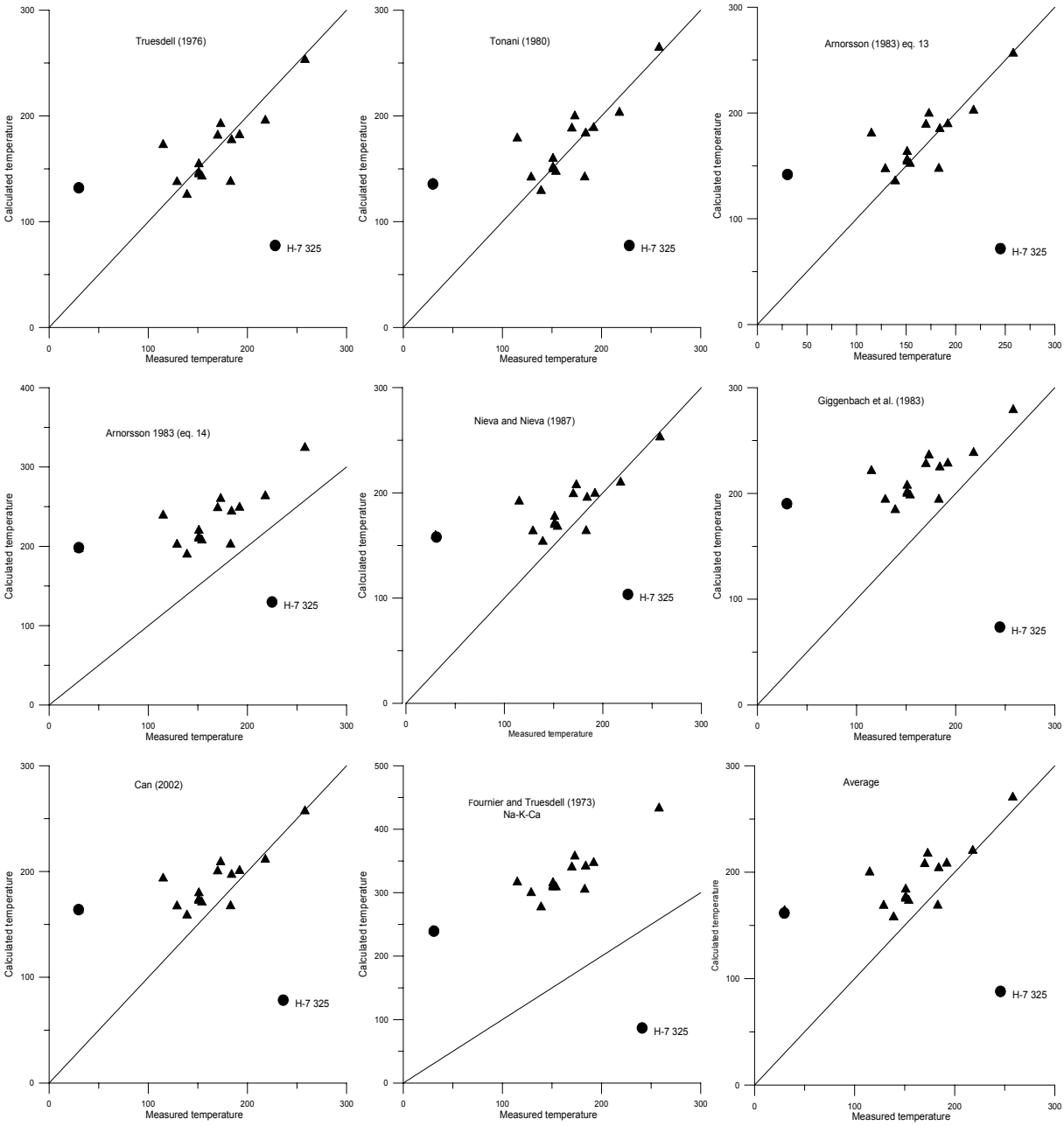

FIGURE 10: Correlation diagrams of measured vs. calculated temperature (in °C) for various Na-K geothermometers for Krýsuvík water samples

high computed temperatures using the Na-K-Ca geothermometer for the water samples from Krýsuvík are explained by calcite precipitation due to boiling in the upflow zone. Figure 10 shows correlation diagrams of measured versus calculated temperature for the Krýsuvík samples for various Na-K geothermometers.

Na-K-Mg ternary diagram and log SiO_2 versus log K^2/Mg equilibrium diagrams

It can be seen from Figure 11 that the range of Na/K ratios is relatively restricted; the $T_{K\text{-}Na}$ values of most samples range between 220 and 280°C. This is consistent with the relatively good agreement of the Na-K geothermometers with measured temperatures (Figure 10). The Mg concentrations in the samples are, on the other hand, highly variable, resulting in a wide range of $T_{K\text{-}Mg}$ values, from close to 0 to more than 200°C. High Mg concentrations are probably a result of mixing with groundwater. This is supported by the fact that the springs and hot water samples from the top part of the wells are concentrated close to the Mg-corner, indicating a typical shallow water origin. Two well samples

TABLE 6: Results of cation geothermometers for the Krýsuvík water samples

Sample	TM[1]	Tr[2]	F[3]	To[4]	A[5]	Nie[6]	Gig[7]	A[8]	Can[9]	NKC[10]	Average
S 1		169	210	175	177	189	219	235	191	270	197
S 2		167	209	173	175	187	217	233	189	258	195
H-3 300	115	173	213	179	181	192	221	239	193	316	200
H-5 200	173	192	230	200	199	207	236	260	209	357	217
H-5 350	154	143	188	147	152	168	198	208	171	309	173
H-5 470	151	147	191	151	156	171	201	212	174	311	177
H-5 650	151	145	190	150	154	170	200	210	173	309	175
H-5 800	151	154	198	160	163	177	207	220	180	315	184
H-6 200	183	138	184	142	147	164	194	202	167	305	169
H-6 500	258	253	278	264	256	253	279	324	257	433	270
H-6 800	218	196	232	203	202	210	238	263	211		220
H-7 325	30	132	179	136	142	159	190	197	163	240	164
H-7 475	139	125	173	129	135	154	184	190	159	277	158
H-8 240	129	138	184	142	147	164	194	202	167	300	169
H-8 450	192	182	221	189	190	199	228	249	201	347	208
H-8 700	184	177	217	184	185	195	225	244	197	341	204
H-8 920	170	182	221	188	189	199	228	248	200	340	208
H-14		211	245	220	217	222	250	280	224	404	234

[1] Measured temperature; [2] Truesdell (1976); [3] Fournier (1979);
[4] Tonani (1980); [5, 8] Arnórsson et al. (1983) - Equations 13 and 14;
[6] Nieva and Nieva (1987); [7] Giggenbach et al. (1983); [9] Can (2002);
[10] Na-K-Ca geothermometer (Fournier and Truesdell, 1973).

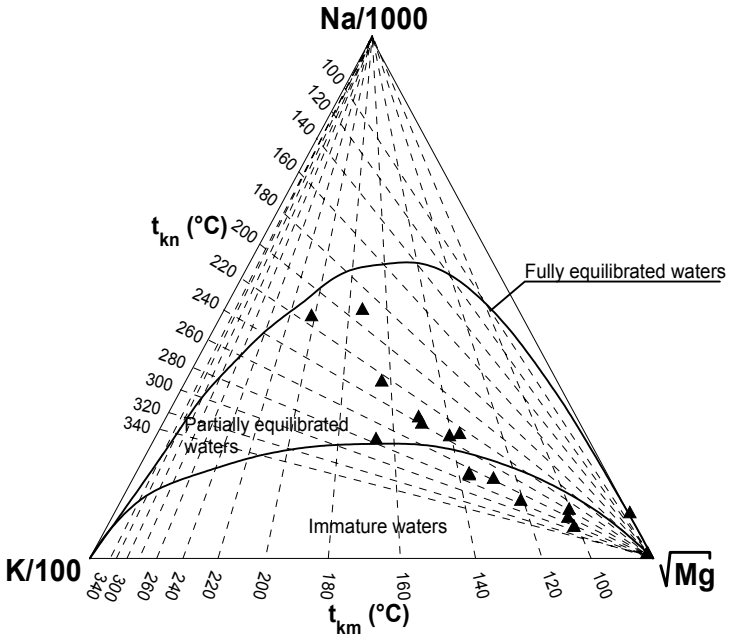

FIGURE 11: Na-K-Mg equilibrium diagram for Krýsuvík water samples

representing samples of well H-6 are plotted close to the field of equilibrium. The Krýsuvík water samples were also plotted on the log (SiO_2) versus log (K^2/Mg) mineral equilibrium diagram (Giggenbach et al., 1994). All the samples lie on the adiabatic cooling zone (Figure 12).

Gas geothermometers

The various geothermometers discussed in Section 3.2.5 were applied to determine subsurface temperature for the Krýsuvík area (Table 7). The agreement of the seven geothermometers was not very good as predicted temperatures commonly varied by about 70ºC for individual samples. However, the discrepancy between the gas geothermometers was more or less constant for different samples, i.e., most of the geothermometers predicted similar differences between the hot and cold samples (Figure 13). The results of the H_2 geothermometer was generally close to the average of other gas geothermometers, ranging between 193 and 270°C with an average value of 238°C, in good agreement with measured temperatures and results of solute geothermometers. For some samples (3, 4, 8, 9 and 10), the calculated values of the H^2/Ar geothermometer are higher than for other gas geothermometers. Arnórsson and Gunnlaugsson's

(1985) CO_2 geothermometer predicted very consistently high temperatures and did not show any correlation with the results of other gas geothermometers. The results of the H_2 geothermometer was generally close to the average of other gas geothermometers if the CO_2 and H_2S values are disregarded, ranging between 193 and 270°C with an average value of 238°C in good agreement with measured temperatures and results of solute geothermometers. Five of the samples; 5, 13, 18, 21, and 22 have consistent low calculated temperatures with an average of 219, 228, 216, 215, and 207°C, respectively.

On the log (XH_2/XAr) versus log (XCO_2/XAr) plot of Giggenbach (1991), most of the Krýsuvík samples plot on the equilibrium vapour (Figure 14). Five samples, however, plotted on the equilibrium liquid. The temperature ranges approximately from 100 to 200°C with only one sample giving 250°C, these values are lower than for the gas geothermometers.

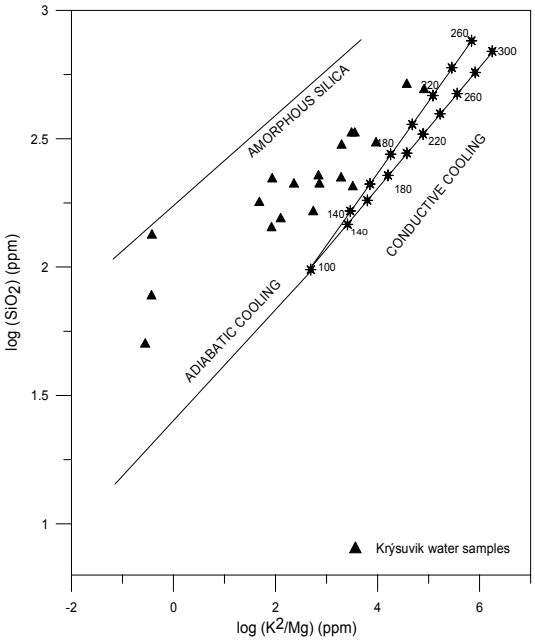

FIGURE 12: Log concentration of SiO_2 versus K^2/Mg equilibrium diagram

TABLE 7: Results of gas geothermometers for Krýsuvík samples

Sample	CO_2[1]	H_2S/H_2[1]	H_2S[1]	H_2[1]	CO_2/H_2[1]	AP[2]	H_2/Ar[3]	Average
1	296	281	278	252	216	179	317	260
2	293	276	277	246	208	292	306	271
3	296	288	279	259	227	309	332	284
4	291	292	272	259	232	312	332	284
5	294	241	250	196	120	204	230	219
6	285	290	259	249	221	297	300	271
7	292	293	268	257	229	298	249	269
8	294	319	245	270	248	293	329	285
9	290	294	253	249	217	296	332	276
10	292	295	250	249	214	289	336	275
11	294	288	254	244	204	286	319	270
12	294	290	252	245	205	278	294	265
13	292	252	252	208	144	217	232	228
14	293	284	262	245	206	284	316	270
15	293	285	257	244	204	282	297	266
16	294	293	249	246	207	265	277	262
17	295	280	257	238	193	270	295	261
18	297	260	231	204	130	193	193	216
19	290	279	257	237	196	282	302	263
20	306	280	247	233	171	222	246	244
21	266	268	200	193	142	203	230	215
22	285	277	195	199	135	176	181	207
Seltún (S)	289	280	279	252	221	308		272
Hveradalur(H)	282	276	263	238	205	287		259
23	328	266	298	248	175		187	250

[1] Arnórsson and Gunnlaugsson (1985); [2] D´Amore and Panichi (1980);
[3] Giggenbach (1991).

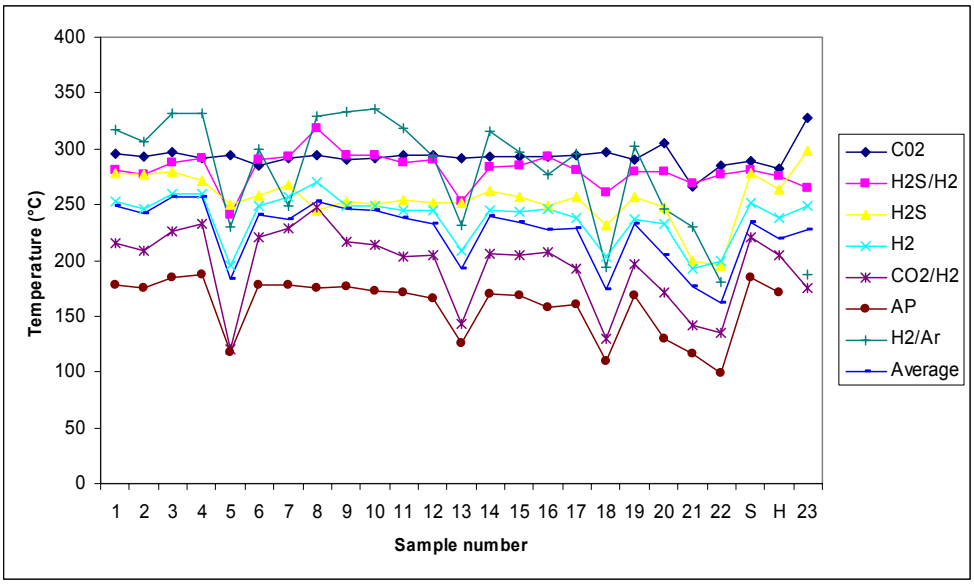

FIGURE 13: Results of the various gas geothermometers for the Krýsuvík area

4.7 Mineral saturation at Krýsuvík

Attempts have been made to reconstruct aluminium composition of the water samples from Krýsuvík by assuming equilibrium between the solution and selected Al-bearing minerals following the FIXAL method of Pang and Reed (1998). Microcline and low albite are the base minerals chosen to fix the aluminium contents of the waters in the FIXAL method and are the main mineral assemblage in the aqueous solution for the experiment of the various cation geothermometers (Chiodini et al., 1991). Furthermore, these minerals are generally close to equilibrium in the geothermal fluids above 200°C in Icelandic as well as in other geothermal systems world wide (Stefánsson and Arnórsson, 2000). The presence of these minerals as secondary phases has been established in Hengill geothermal systems (Larsson et al., 2002). The saturation index for aluminium-bearing minerals shifts towards undersaturation with decreasing concentration of aluminium and oversaturation with increasing aluminium concentration.

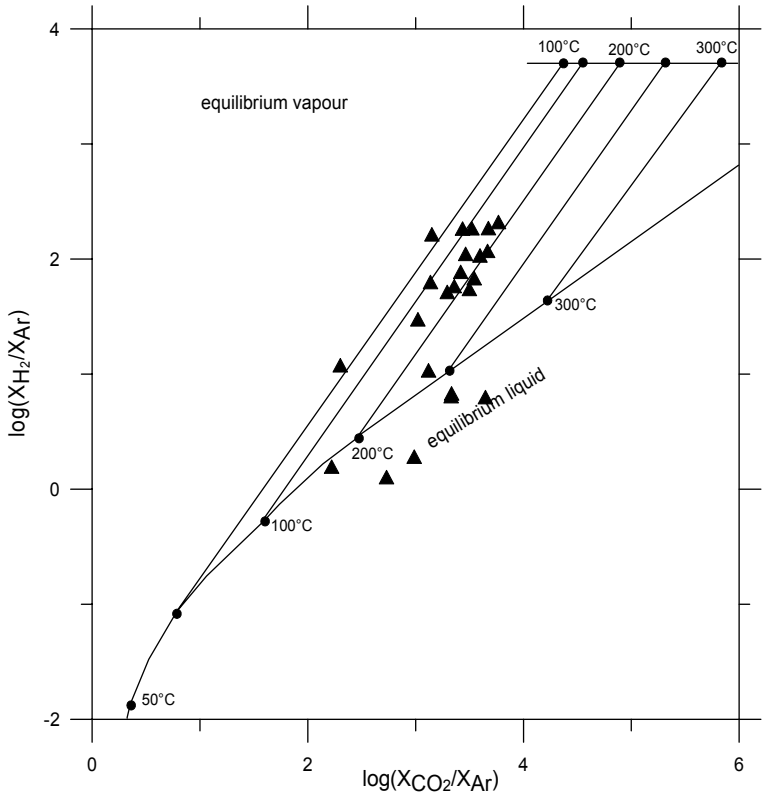

FIGURE 14: Log (X_{H2}/X_{Ar}) versus log (X_{CO2}/X_{Ar}) equilibrium plot for Krýsuvík gas samples

Aluminium was fixed by successively changing aluminium concentration of a given water sample until the saturation indices of the selected minerals converged at saturation. A little change in the aluminium concentration also slightly affects the saturation state of the aluminium free minerals such

as calcite and anhydrite. Saturation plots were not prepared for all wells due to chloride deficiency to balance the cations; such as samples from H-5 and H-7. The absence of sodium analysis also prevented the use of H-3 200. The equilibrium diagrams for the samples are presented as saturation index versus temperature in Figures 15 and 16.

The saturation diagrams for well H-6 indicate a systematic discrepancy of equilibrium temperature with respect to measured temperature. For samples H-6 200, 500 and 800, the measured temperatures are equal to 183, 258, and 218°C whereas the corresponding mineral equilibrium temperatures are equal to 200, 274, and 225°C, respectively. The convergence corresponds to equilibrium with microcline, quartz and low albite and slight supersaturation with respect to anhydrite and montmorillonite. Calcite is oversaturated at 200 and 500 m at the whole range of temperatures and above 100°C at 800 m, where as most of the samples are undersaturated with respect to anhydrite except for the high temperature ones.

The discrepancy between measured temperatures and temperatures using the mineral equilibrium method is relatively high for well H-8 with equilibrium temperatures of 217 and 230°C compared to measured temperatures of 170 and 184°C for samples H-8 920

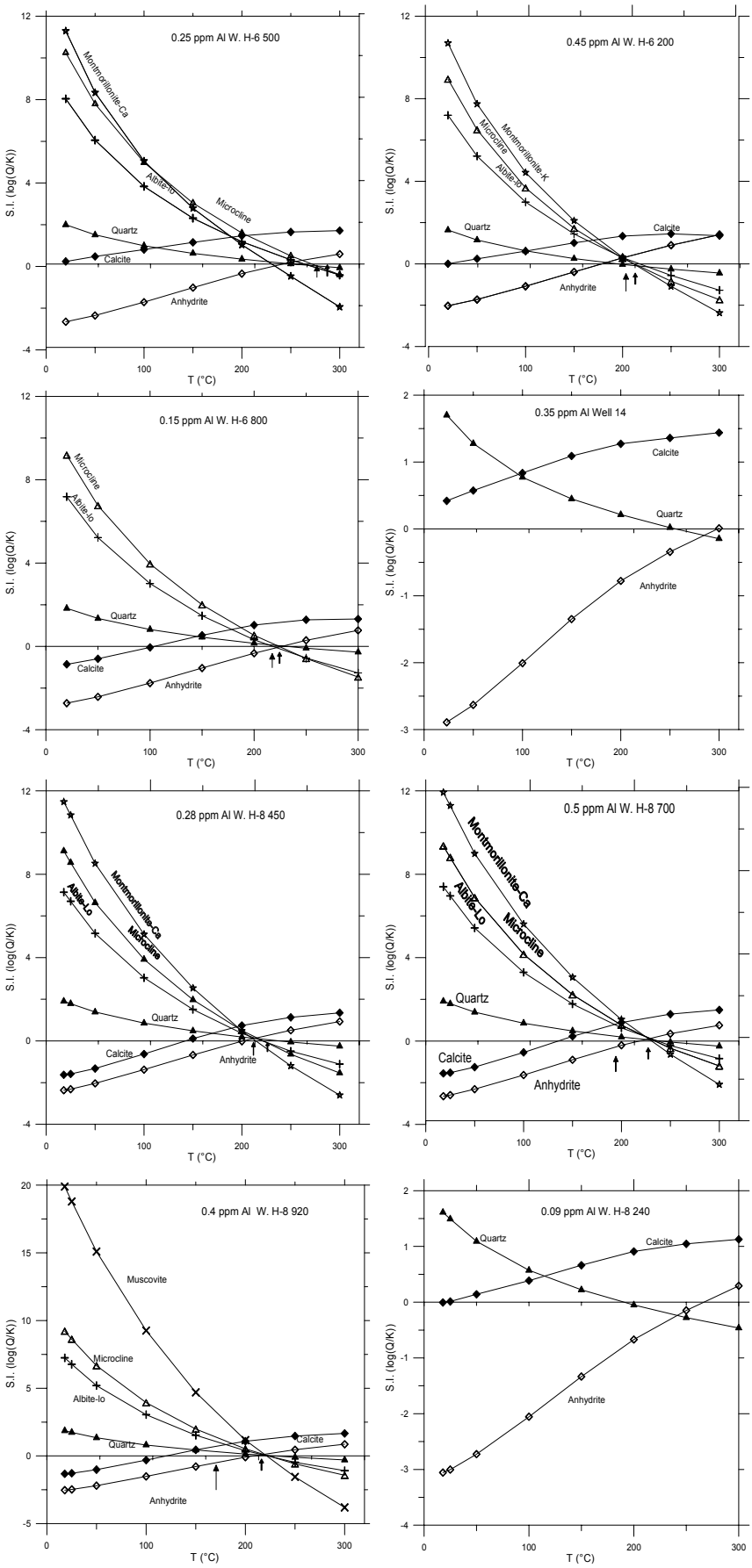

FIGURE 15: Mineral equilibrium diagrams for samples from wells H-6, H-8, and 14 in Krýsuvík

and H-8 700, respectively. However H-8 450 has only a slight temperature difference, with 192 and 210°C for the measured and equilibrium temperatures, respectively. Perfect convergence with montmorillonite, microcline, low albite, quartz and anhydrite marks the equilibrium temperature of samples H-8 700, H-8 450 and H-8 920.

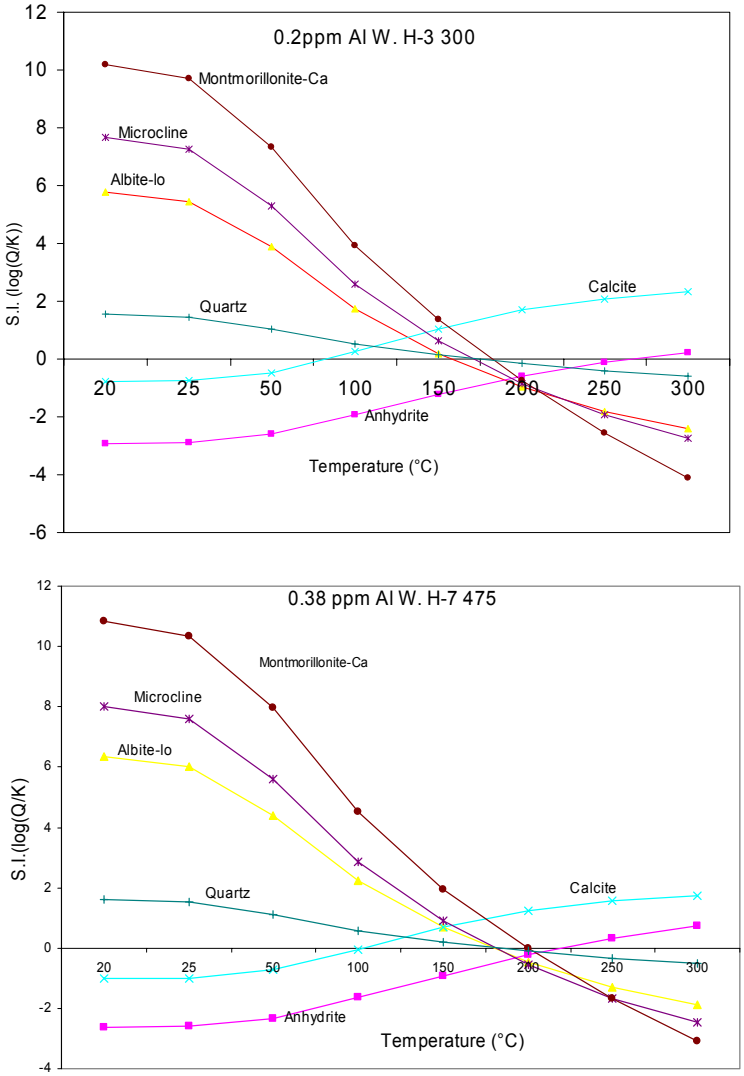

FIGURE 16: Mineral equilibrium diagrams for well samples H-3 300 and H-7 475 in Krýsuvík

4.8 Mixing models

The Na-K-Mg ternary diagram (Figure 11) provides a clue to whether geothermal water samples have been affected by mixing with ground water. Samples that fall in the immature field of Figure 11 do not represent equilibrium conditions and are generally interpreted to have been affected by mixing with cold water, as Mg concentration decreases dramatically with increasing temperature (Fournier and Potter, 1979). The Krýsuvík samples define a linear array in Figure 11 on radiating out of the Mg corner. This is an indication that the cold water contribution is higher in the samples plotted towards the Mg corner. The discrepancy of measured and calculated temperature could also be a result of the mixing.

A silica-enthalpy mixing model was used to evaluate the effect of this process (Figure 17). A cold water sample for the mixing end member was taken from VL4 cold water well with silica composition of 17.1 mg/kg and temperature of 21°C (Flóvenz et al., 1986). Two lines of mixing are constructed through the data set. Line A is the mixing line that connects the cold water with the maximum measured temperature and, thus, a high silica content. Line B corresponds to the best fit line that takes into consideration almost all the samples. The water enthalpies at the intersection of line A and line B with the quartz solubility curve are 1171 and 971 kJ/kg, respectively, corresponding to estimated reservoir temperatures of 269 and 227°C.

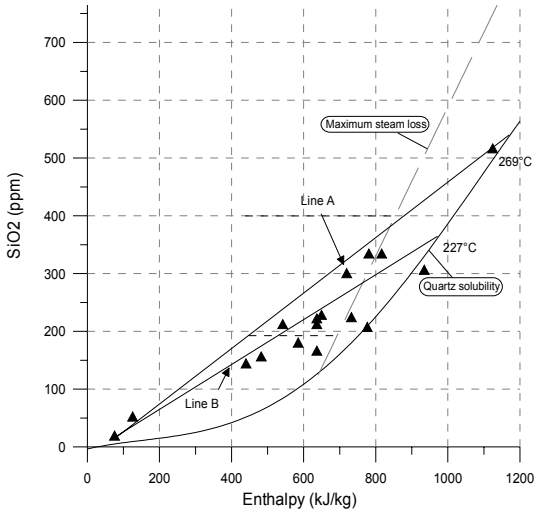

FIGURE 17: Silica mixing model for Krýsuvík water well samples

5. ALID GEOTHERMAL FIELD, ERITREA

5.1 Geology of Alid

Alid is part of the Danakil depression, a region of active volcanism and high heat flux. Alid volcanic centre is located on the axis of the rift zone that radiates north-northwest from the main triple junction of the Afar triangle (Lowenstern et al., 1999). Alid Mountain is located in a depression bounded by the Danakil horst to the east and the Eritrean plateau to the west. The Precambrian basement and granites are covered with Mesozoic to Tertiary sediments and Tertiary basalts. Pliocene to Quaternary rift succession mainly lavas and minor sediments cover the Danakil depression.

Alid volcanic centre is an elliptical dome that rises up to 700 m above the adjacent plains of the Danakil depression (Figure 18; Clynne et al., 1996). The oldest rock of the Alid volcanic centre is a Precambrian mica- and kyanite-schist that crops out only in a small area of the dissected canyon that drains the east side of the mountain. Sedimentary succession consisting mainly of marine siltstones and sandstones, gypsum beds, fossiliferous limestones, and pillow basalts, and sub-aerial basalts overlie the basement. All these lithologies are inferred to be of Pleistocene or possibly Pliocene age.

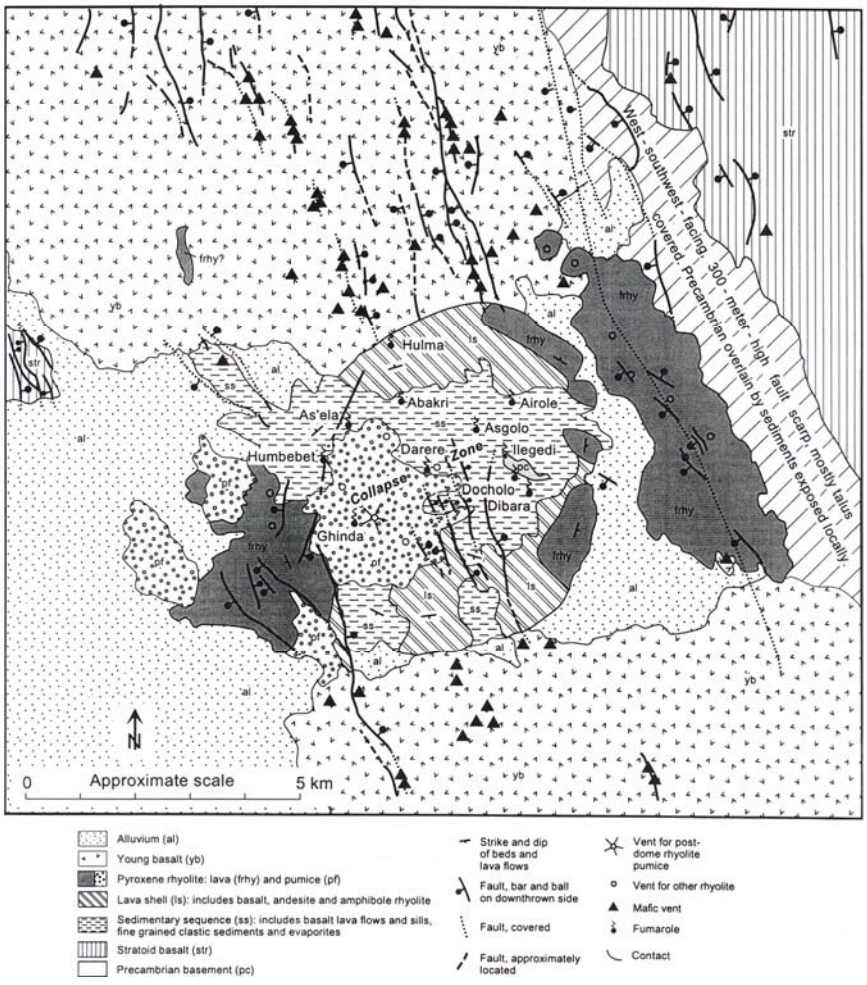

FIGURE 18: Geological map and sample location map of Alid volcanic centre (Clynne et al., 1996)

Up to 1000 m of structural doming, which began less than about 36 thousand years ago caused considerable swelling of the dome and resulted in land sliding and collapse of the central region. Fractures associated with this deformation are apparent on aerial photographs. The north-northwesterly faults are in agreement with the major structural trend of the rift.

5.2 Geothermal manifestations

Surface manifestations of geothermal activity in the area include fumaroles, pools and hot springs. Eleven geothermal sites have been identified, six of which were selected for sampling of gas and water (Lowenstern et al., 1999). Ilegedi, Darere and As´ela are the most important ones with the first being the largest and most prominent. Owing to lack of fumarolic venting, Ghinda, Docholo and Dibara

were not sampled although the respective temperatures of springs reach 93, 90, and 80°C. The fumaroles and boiling pools occur in all lithological units, in rhyolithic breccia at Abakri, As´ela, and Darere, the sedimentary sequence at Humbebet, and in the Precambrian basement rocks at Ilegedi. Thus the various lithological units do not seem to control the distribution of the geothermal surface manifestation. However, the geothermal activity appears to be controlled by fractures as most of the fumaroles and alteration zones occur in alignments.

White and red clays, white and yellow crustose sublimates and fine grained white and green sublimates are the most common surface alteration products. The sublimate minerals are found to be ammonium hydrates and sulphates (Beyth, 1996). Anhydrite, Kalinite/alum [$KAl(SO_4)_2.11H_2O$], tchermigite [$(NH_4)Al(SO_4)_2.12H_2O$], montmorillonite, and illite are among the most common alteration minerals.

5.3 Chemical composition of Alid samples

Table 8 lists the chemical analyses of the water samples from Alid. These hydrothermal samples collected at Alid are from pools except for sample ELW96-10 from Humbebet, which is a drip. Data obtained from gas analyses are reported in Table 9. All of the samples contained over 95% H_2O except for the bubbling pool of Ilegedi 3 (sample ELG96-5) where significant condensation had occurred.

TABLE 8: Chemical composition of Alid water samples in ppm

Sample	Locality	T(°C)	pH	SiO_2	Na	K	Ca	Mg	Li	NH_4
ELW96-5	Ilegedi 1	50	5	195	18.2	11.4	101	31.2	0.02	213
ELW96-6	Ilegedi 2	35	3	402	18.3	132	114	23.5	0.02	105
ELW96-7	As´ela 1	54	7	114	233	20	396	27.2	0.05	15.9
ELW96-8	As´ela 2	57	7	71	213	17	251	21.7	0.04	5.8
ELW96-9	Ilegedi 3	66	6	99.1	11.4	12	157	37.4	0.02	190
ELW96-10	Humbebet	<60	7	39.8	2.86	1.18	111	10.2	0	30.4
Cold water	Buya well	33		54.3	69.7	32.7	126	73.9	0.1	0.1

Sample	Fe	Mn	Cl	SO_4	HCO_3	F	B	TDS
ELW96-5	10.1	3.11	2.99	1094	0	0.45	0.022	1695
ELW96-6	19.7	3.2	1.19	1767	0	0.21	0.031	2606
ELW96-7	0.04	0.56	20.9	1475	100	0.49	0.049	2417
ELW96-8	0.17	0.24	12.4	1068	66	0.43	0.044	1748
ELW96-9	0.82	3.04	0.84	949	171	1.18	0.015	1633
ELW96-10	<.01	<.01	0.14	74.3	263	0.04	0	572
Cold water	<.01	<.01	59	458	258	0.99	0.33	1195

TABLE 9: Chemical composition of gas samples from Alid (mole % gas and gas/steam ratio)

Sample	CO_2	H_2S	H_2	CH_4	N_2	Ar	Gas/steam[1]
ELG96-2	97.93	0.219	1.093	0.225	0.412	0.0054	0.0448
ELG96-3	95.53	0.876	2.498	0.132	0.598	0.0126	0.0196
ELG96-4	98.2	0.749	0.503	0.061	0.473	0.0116	0.0259
ELG96-5	95.89	0.662	2.624	0.144	0.653	0.014	1.701
ELG96-6	98.89	0.143	0.605	0.085	0.209	0.0047	0.0565

[1] Gas/steam molar ratio of total gas divided by moles H_2O

Since the chloride content is low, ranging from 0.14 to 20.9 ppm, it is advisable to use the anion Cl-SO_4-HCO_3 ternary diagram (Figure 19) as the basis of initial classification (Giggenbach, 1991). According to it, the Alid water samples, are classified as steam heated water, with one exception that falls in the field of HCO_3- rich waters. This is consistent with low pH values of water (ELW96-5 and 6 with respective pH values of 5 and 3). The high SO_4^{2-} content and low pH of steam-heated water is a result of near surface oxidation of H_2S proceeding from a deep reservoir zone resulting in the formation of H_2SO_4 (sulphuric acid).

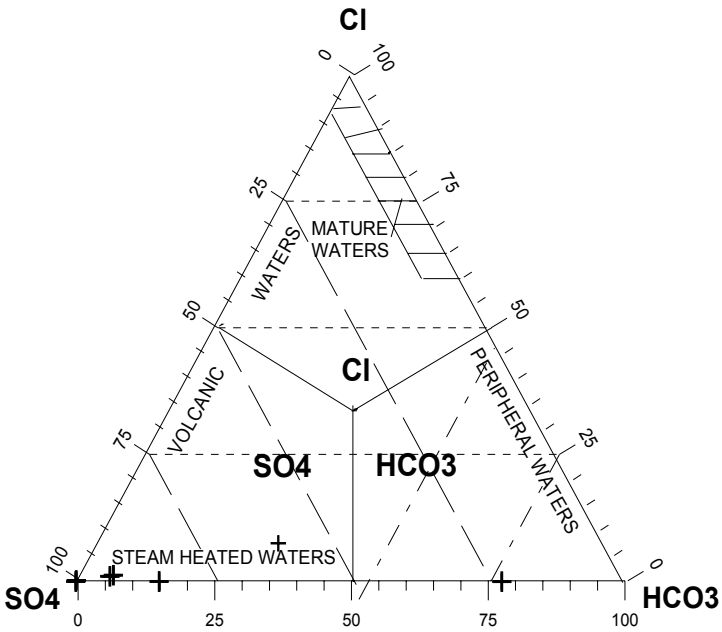

FIGURE 19: Cl-SO_4-HCO_3 ternary diagram for classification of Alid water waters

Binary plots of Alid water samples, presented in Figure 20, illustrate some of the characteristics of steam-heated waters. The Cl concentrations of the water samples are very low, ranging from 0.14 to 21 ppm whereas the concentrations of other elements do not exhibit any systematic trends. The Na versus chloride plot shows a possible positive correlation of these elements. The line fit for this molar plot corresponds to a Cl/Na ratio of about 0.1 or significantly below the halite dissolution line (Cl/Na ratio 1) and far below the Cl/Na ratio of sea water – meteoric

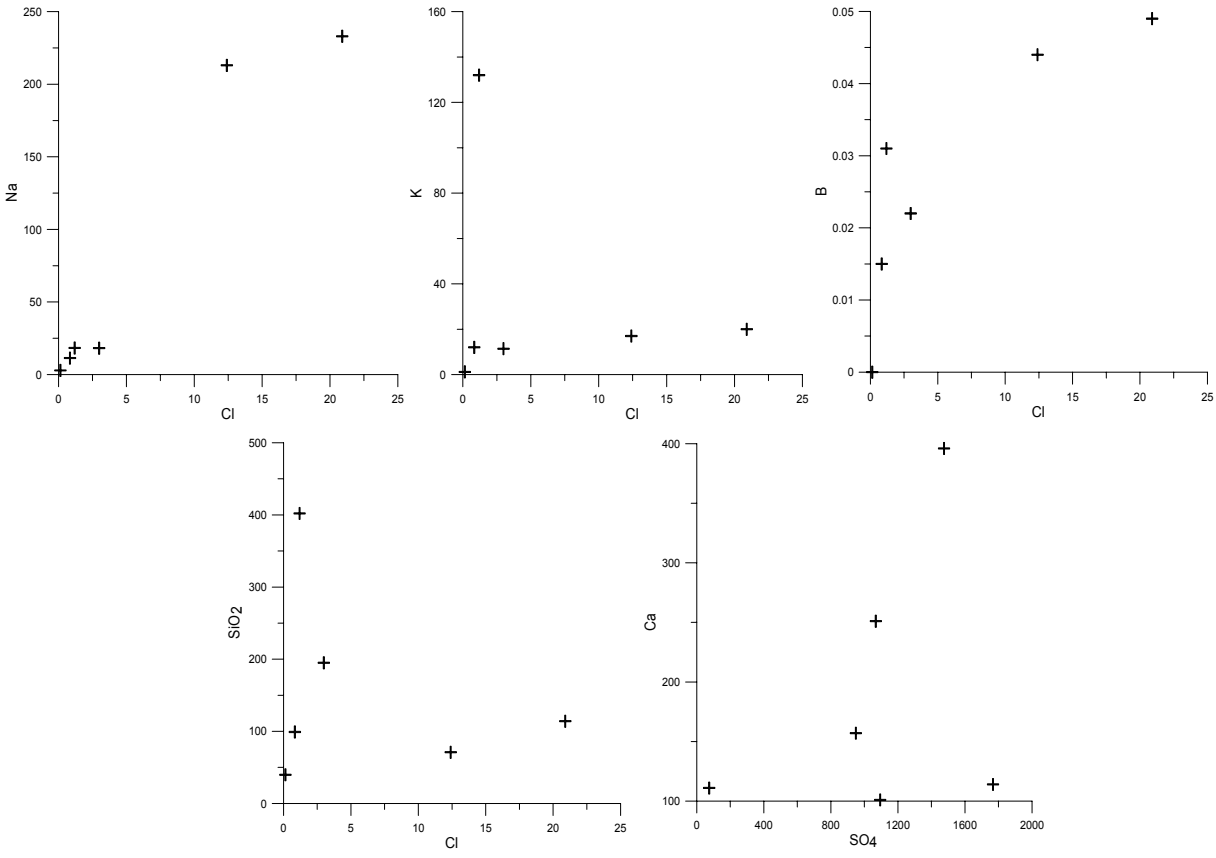

FIGURE 20: Binary plots of Cl vs. cations, B and SiO_2 and SO_4 vs. Ca, units are in ppm

water mixing line (1.2; Minissale et al., 2003). Chloride is a conservative component in geothermal solutions, i.e., the concentration of this element will increase continuously during progressive rock dissolution. The very low Cl concentrations indicate that the fluids have not interacted extensively with the bedrock, i.e., they do not represent mature geothermal fluids. Elevated concentrations of other components are due to rapid dissolution of the bedrock in the highly acidic steam-heated waters, i.e., they do no represent equilibrium concentrations corresponding to some reservoir conditions but rather the extent of bedrock dissolution that has occurred at the surface. Consequently, the application of solute geothermometers, mineral saturation calculations, and mixing models to the surface solutions from Alid will not provide information on the conditions in the underlying geothermal reservoir. However, it can be informative to compare predicted reservoir temperatures for Alid using gas geothermometers to those predicted by solute geothermometers in order to evaluate the magnitude of the potential error that could result from mistaking steam-heated surface waters for deep geothermal solutions.

5.4 Geothermometry of Alid gas and water samples

As noted above, the natural geothermal solutions that are available on the surface at Alid are dominated by acid sulphate waters; therefore the gas geothermometers present the best methods for predicting subsurface reservoir temperatures (Goff and Janik, 2000). The calculated values of the geothermometers are presented in Table 10 and depicted in Figure 21. The CO_2 value and H_2/Ar of Arnórsson and Gunnlaugsson (1985) and Giggenbach (1991), respectively, display similar results which are higher than for other gas geothermometers. One sample, from the bubbling pool, has a calculated temperature of 561°C using the CO_2 geothermometer. This extremely high value is due to steam condensation in the pool, which dramatically increases the gas/steam ratio. The average gas thermometer temperatures for the samples (excluding the sample from the bubbling pool) range from 256 to 281ºC. The calculated values using the CO_2/H_2 of Arnórsson and Gunnlaugsson (1985) and D´Amore and Panichi (1980) geothermometers are quite low ranging, respectively, from 164 to 207°C and 206 to 263°C.

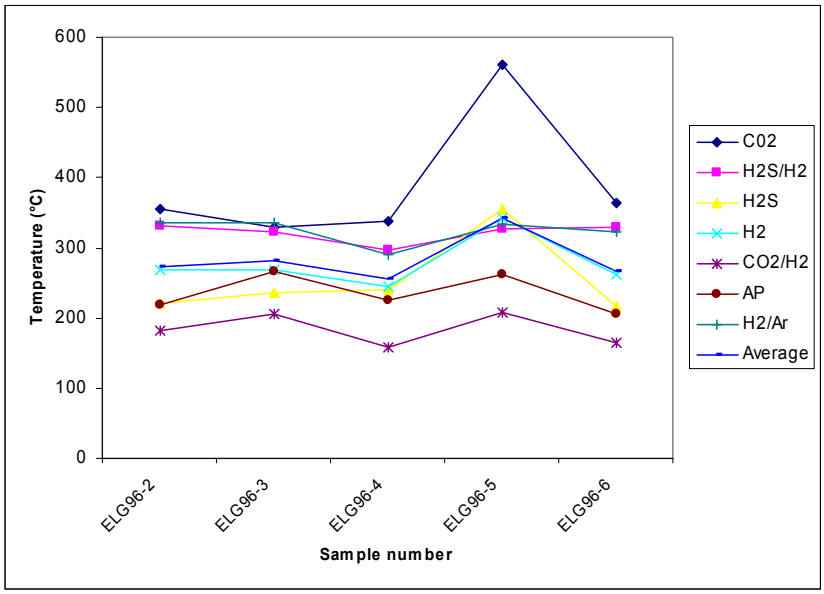

FIGURE 21: Scatter plot of gas geothermometers of Alid gas samples. The CO_2, H_2S, H_2, and CO_2/H_2 are geothermometers from Arnórsson and Gunnlaugsson (1985); AP is D'Amore and Panichi (1980), and H_2/Ar is the Giggenbach (1991) geothermometer

The six gas samples of Alid were plotted in the CO_2-Ar versus H_2-Ar equilibration diagram (Figure 22; Giggenbach, 1991). All of them plot in the vapour equilibrium zone. This indicates that the anticipated underlying hydrothermal system is a vapour-dominated, high-enthalpy geothermal reservoir. The predicted temperatures range from 200 to 275°C, which is in reasonable agreement with the average gas geothermometer temperatures.

TABLE 10: Results of gas geothermometers for Alid samples

Sample	CO_2[1]	H_2S / H_2[1]	H_2S[1]	H_2[1]	CO_2 / H_2[1]	AP[2]	H_2/Ar[3]	Average
ELG96-2	356	332	221	268	181	218	336	273
ELG96-3	330	322	237	268	206	266	336	281
ELG96-4	339	297	240	245	159	225	290	256
ELG96-5[4]	561	328	355	343	207	263	334	342
ELG96-6	364	329	216	262	164	206	323	266

[1] Arnórsson and Gunnlaugsson (1985);
[2] D´Amore and Panichi (1980);
[3] Giggenbach (1991);
[4] Bubbling pool.

Silica geothermometers were applied to the Alid water samples. The results are shown in Table 11 and depicted on Figure 23. Inspection of Table 11 shows that the average predicted silica temperatures of the surface samples range from 87 to 225°C. This is significantly lower than predicted by the gas geothermometers as expected, considering the steam-heated nature of the Alid water samples. It is interesting to note that the two samples that yield the highest silica temperatures, ELW96-6 and ELW96-5 do also have the lowest pH values, 3 and 5, respectively. This is further evidence for the steam-heated nature of these waters and illustrates that the high silica concentration of these samples is due to rapid rock dissolution in the very acidic environment, but not equilibrium with quartz at high temperature.

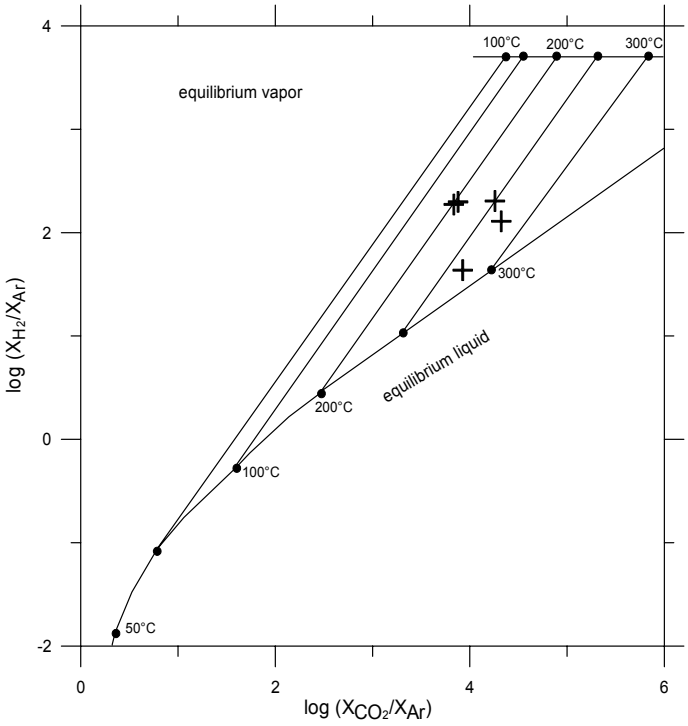

FIGURE 22: Alid gas samples plot showing log concentration of CO2/Ar vs. H2/Ar equilibrium diagram

TABLE 11: Results of selected silica geothermometers for Alid samples

Samples	F [1]	F [2]	FP[4]	A[5]	A[6]	VS[7]	Average	F[8]	A[9]
ELW96-5	178	167	173	170	159	179	171	157	151
ELW96-6	233	211	229	234	210	233	225	222	209
ELW96-7	145	139	139	133	129	145	138	119	117
ELW96-8	119	117	114	106	105	119	113	90	90
ELW96-9	137	132	132	125	122	137	131	110	108
ELW96-10	91	94	88	77	79	92	87	61	63

[1] Measured temperature;
[2,3] Fournier (1977) Equations 1 and 2, respectively;
[4] Fournier and Potter, (1982);
[5,6] Arnórsson, (2000) Equations 4 and 5, respectively;
[7] Verma and Santayo (1997);
[8] Chalcedony (Fournier, 1977);
[9] Chalcedony (Arnórsson et al., 1983).

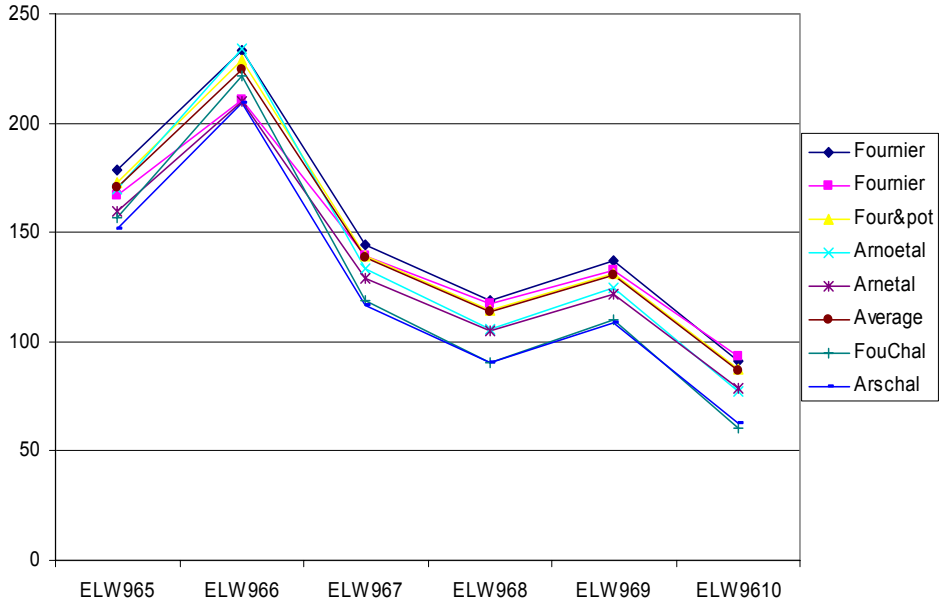

FIGURE 23: Calculated temperatures of Alid water samples with the response of the various silica geothermometers. The two Fourniers represent Equations 1 and 2, respectively, in Fournier (1977); Four & Pot is Fournier and Potter (1982); Arnoetal is Equation 5 in Arnórsson (2000); Arnetal is Equation 6 in Arnórsson (2000); FouChal is the Chalcedony equation - Equation 9 in Fournier (1977); and Arschal is Arnórsson et al. (1983)

6. CONCLUSIONS

The relationship of the various geothermometers versus measured temperature allows differentiating the suitable geothermometers and predicting the various processes such as mixing conditions in the Krýsuvík wells. The temperature attained from the mineral equilibration method likely approaches the measured temperature and systematically changes with temperature decline or increase. The correspondence of calculated and measured temperature indicates that mixing of cold and hot fluids at different levels of the reservoir did not influence well H-6 at Krýsuvík, at the time of sampling. The discrepancy of calculated and measured temperatures in well H-8 may, on the other hand, be caused by mixing of hot and cold water from various levels. The 47°C temperature difference in the bottom part of the well (920 m) could indicate that hot water flows from the upper (450 m) aquifer to the bottom. Thus, the main reason of inconsistency of the aquifer temperature and equilibrium temperatures is that there are several feeding aquifers with different temperatures. This is supported by the observed inverse temperature profiles in most wells. It is also found out that the quartz geothermometers of Fournier (1977) Equation 2, and Fournier and Potter (1982), as well as Verma and Santayo, (2000) and Arnórsson et al., (2000) Equation 4, and Na-K geothermometers of Tonani (1980) Equation 12, Arnórsson et al. (1983) Equation 13 and Truesdell and Fournier (1976) Equation 11 geothermometers are considered to give reasonable estimates of sub-surface temperature.

Gas geothermometer temperatures for Krýsuvík gave systematically inconsistent results. However, the average values of the several gas geothermometers for individual samples predicted subsurface temperatures that were generally in the same range as predicted by the solute geothermometers and observed by direct measurements. The H_2 gas geothermometer of Arnórsson and Gunnlaugusson (1985) was generally very close to the average of the other geothermometers. The constant results of the CO_2 and H_2S did not perform well at Krýsuvík. The calculated temperature using the $\log(X_{H_2}/X_{Ar})$

versus log(X_{CO_2}/X_{Ar}) plot of Giggenbach (1991) for Krýsuvík samples displayed lower temperature values than other gas geothermometers with a temperature range from 100 to 220°C with only one sample predicting 250°C.

Although the distribution is uneven, contouring of isothermal lines was plotted for the Krýsuvík and Trölladyngja areas (Figure 24). An oval shaped temperature anomaly close to Krýsuvík and an open anomaly close to Trölladyngja are conspicuously displayed. The Krýsuvík anomaly shows a E-W direction despite the dominantly NE-SW orientation of the tectonic and volcanic features, such as the Sveifluháls hyaloclastite ridge. The outline of this anomaly closely overlaps with the resistivity anomaly close to sea level (Figure 4). It can, therefore, be anticipated that the anomaly may be associated with an E-W trending structure or a permeable zone that hosts the geothermal reservoir. The open anomaly close to Trölladyngja correlates well with the Vesturháls hyaloclastite ridge. It also fits with the Schlumberger anomaly of Georgsson (1987) and the northern extension of the open anomaly at 150 m a.s.l. of Ha Ngoc Hung (1997) (Figure 4).

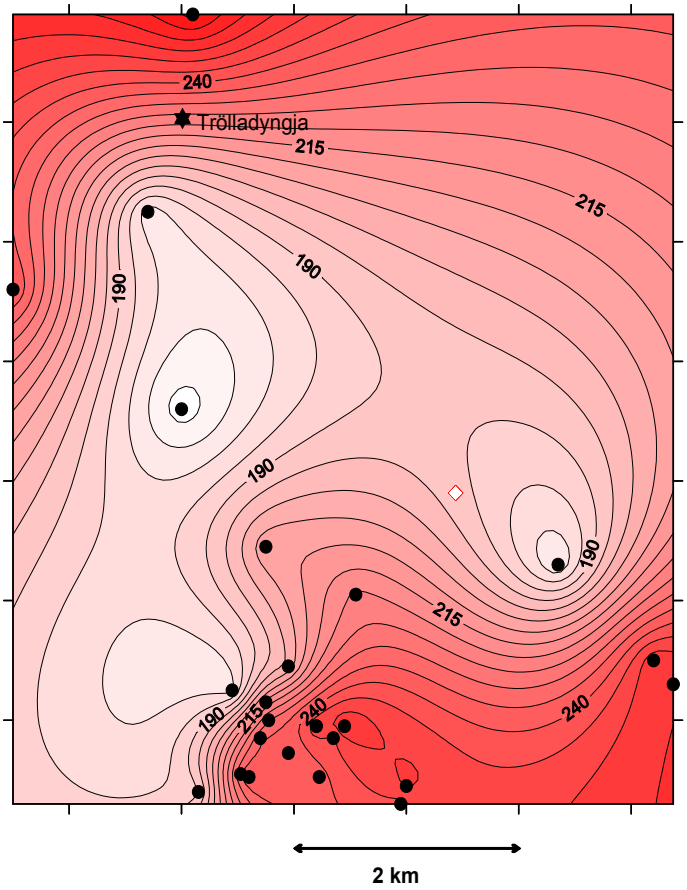

FIGURE 24: Isothermal lines in the Krýsuvík area; the Krýsuvík locality is slightly out of the area towards south

The Alid water samples are characterized by low pH and high sulphate content, typical of steam heated surface waters. As a result, solute geothermometers do not represent temperatures of the geothermal reservoir. This is reflected by low quartz-geothermometer temperatures (80 to 224ºC) compared to the gas-thermometer temperatures that range between 163 and 364 with an average of 272ºC. The results indicate that the geothermal reservoir at Alid is vapour-dominated and surface thermal waters derive from shallow, steam-heated ground water reservoirs.

In order to visualize the underground conditions of Alid, a conceptual model is proposed based on the geochemical results so far outlined (Figure 25). Meteoric water as a source (Lowenstern et al., 1999) descends down deep into the reservoir and magma heats it mainly by conduction and probably convection with some elements, where the vapour-dominated phase in turn heats the aquifer above which develops into a steam-dominated zone. The water rises up towards the surface as fumaroles or hot springs along the main fracture system mixed with the ground water.

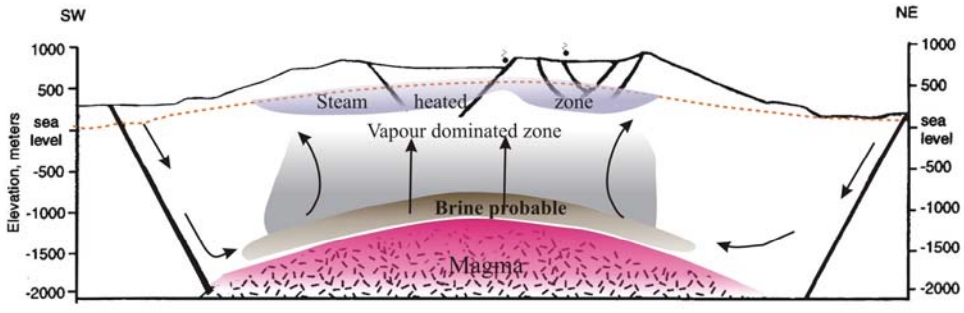

FIGURE 25: Conceptual model of Alid geothermal field based on geochemistry

ACKNOWLEDGEMENT

Praise the almighty God, I would like to thank the UNU and the Icelandic Government for the support extended to the UNU Geothermal Training Programme; Dr. Ingvar Birgir Fridleifsson and Mr Lúdvík S. Georgsson, not only for this great opportunity to attend the training programme but also for the assistance given all through the duration of the course. Special thanks go to Gudrún Bjarnadóttir for her wonderful care in all administrative works. My advisor Dr. Thráinn Fridriksson is acknowledged for his generous and suggestive guidance and help with preparing this report; and Dr. Halldór Ármansson for his generous support in feeding up materials and crucial assistance in tackling geochemical works; all the UNU lecturers for their valuable teaching; and the staff of Orkustofnun and ISOR for continuous support. The librarians are particularly highly acknowledged.

I would like to thank BGR in Germany, and in particular Dr. Michael Kraml, for partially funding my training. My thanks extend to the Department of Mines, Eritrea for allowing me to participate in the training programme. Lastly, thanks extend to my family for their continuous encouragement throughout the duration of the training.

REFERENCES

Ármannsson, H., Thórhallsson, S., and Ragnarsson, Á., 1994: *Krýsuvík-Trölladyngja. Potential steam production and transmission to energy park, Straumsvík*. Orkustofnun, Reykjavík, report OS-94012/JHS-07B, 17 pp.

Arnórsson, S., 1985: The use of mixing models and chemical geothermometers for estimating underground temperature in geothermal systems. *J. Volc. Geotherm. Res., 23,* 299-335.

Arnórsson, S., 1987: Gas chemistry of the Krýsuvik geothermal field, Iceland, with special reference to evaluation of steam condensation in upflow zones. *Jökull, 37,* 31-47.

Arnórsson, S., 1991: Geochemistry and geothermal resources in Iceland, In: D´Amore, F. (co-ordinator), *Applications of geochemistry in geothermal reservoir development.* UNITAR/UNDP publication, Rome, 145-196.

Arnórsson, S., 1995: Geothermal systems in Iceland: Structure and conceptual models II. Low-temperature areas. *Geothermics, 24*, 603-629.

Arnórsson, S. (ed.), 2000: *Isotopic and chemical techniques in geothermal exploration, development and use. Sampling methods, data handling, interpretation*. International Atomic Energy Agency, Vienna*,* 351 pp.

Arnórsson, S., Björnsson, A., Gíslason, G., and Gudmundsson, G., 1975: Systematic exploration of the Krýsuvík high-temperature area, Reykjanes Peninsula, Iceland. *Proceedings of the 2nd U.N. Symposium on the Development and Use of Geothermal Resources, San Francisco, 1,* 853-864.

Arnórsson, S., and Gunnlaugsson, E., 1985: New gas geothermometers for geothermal exploration – calibration and application, *Geochim. Cosmochim. Acta, 49,* 1307-1325.

Arnórsson, S., Gunnlaugsson, E., and Svavarsson, H., 1983: The chemistry of geothermal waters in Iceland. III. Chemical geothermometry in geothermal investigations. *Geochim. Cosmochim. Acta, 47*, 567-577.

Beyth, M., 1996: Preliminary assessment of the Alid geothermal field, Eritrea. *Geological Survey of Israel current research, 10*, 124-128.

Can, I., 2002: A new improved Na/K geothermometer by artificial neural networks. *Geothermics, 31*, 751-760.

Chiodini G., Cioni, R., Guidi, M., and Marini, L., 1991: Chemical geothermometry and geobarometry in hydrothermal aqueous solutions: A theoretical investigation based on a mineral-solution equilibrium model. *Geochim. Cosmochim. Acta, 55*, 2709-2727.

Chiodini, G., and Marini, L., 1998: Hydrothermal gas equilibria: the H_2O-H_2-CO_2-CO-CH_4 system *Geochim. Cosmochim. Acta, Volume 62, 15,* 2673-2687.

Clynne, M.A., Duffield, W.A., Fournier, R.O., Weldegiorgis, L., Janik, C.J., Kahsai, G., Lowenstern, J., Weldemariam, K., and Tesfai, T., 1996: *Geothermal potential of the Alid Volcanic Center, Danakil depression, Eritrea*. U.S. Geol. Survey, final report to U.S. Agency for International Development under the terms of PASA No. AOT-0002-P-00-5033-00, 46 pp.

D'Amore, F., 1991: Gas geochemistry as a link between geothermal exploration and exploitation. In: D'Amore, F. (coordinator), *Application of geochemistry in geothermal reservoir development* UNITAR/UNDP publication, Rome, 93-117.

D'Amore, F., and Panichi, C., 1980: Evaluation of deep temperatures of hydrothermal systems by a new gas geothermometer. *Geochim.Cosmochim. Acta, 44*, 549-556.

Ellis, A.J., and Mahon, W.A.J., 1977: *Chemistry and geothermal systems*. Academic Press, New York, 392 pp.

Ellis, A.J., and Wilson, S.H., 1960: The geochemistry of alkali metals ions in the Wairakei hydrothermal system, *N. Z. J. geol.geophys, 3*, 593-617.

Fahlquist, L., and Janik, C.J., 1992: *Procedures for collecting and analysing gas samples from geothermal systems*. US Geological Survey, open-file report 92-211, 19 pp.

Fiebig J., Chiodini G., Caliro S., Rizzo A., Spangenberg J. and Hunziker J.C., 2004: Chemical and isotopic equilibrium between CO_2 and CH_4 in fumarolic gas discharges: Generation of CH_4 in arc magmatic-hydrothermal systems *Geochim. Cosmochim. Acta, 68,* 2321-2334.

Flóvenz, Ó.G., Fridleifsson, G.Ó., Johnsen, G.V., Kristmannsdóttir, H., Georgsson, L.S., Einarsson, S., Thórhallsson, S., and Jónsson, S.L., 1986: *Vatnsleysa-Trölladyngja, freshwater and geothermal investigation.* Orkustofnun, Reykjavík, report OS-86032/JHD10B, 92 pp.

Fournier, R.O., 1977: Chemical geothermometers and mixing model for geothermal systems. *Geothermics, 5,* 41-50.

Fournier, R.O., 1979: A revised equation for Na-K geothermometer. *Geoth. Res. Council, Trans., 3,* 221-224.

Fournier, R.O., 1985: The behaviour of silica in hydrothermal solutions. *Rev. Econ. Geology, 2,* 45-61.

Fournier, R.O, 1991: Water geothermometers applied to geothermal energy, In: D´Amore, F., (co-ordinator), *Application of geochemistry in geothermal reservoir development.* UNITAR-UNDP Publication, Rome, 37-69.

Fournier, R.O., and. Potter, R.W, 1979: A magnesium correction for the Na–K–Ca geothermometer for natural waters. *Geochim. Cosmochim. Acta, 43*, 1543–1550.

Fournier, R.O., and Potter, R.W., 1982: An equation correlating the solubility of quartz in water from 25° to 900°C at pressures up to 10,000 bars. *Geochim. Ccosmochim Acta, 46*, 1969-1973.

Fournier, R.O. and Rowe, J.J., 1962. The solubility of cristobalite along the three-phase curve, gas plus liquid plus cristobalite. *Am. Mineralogist 47,* 897–902.

Fournier, R.O., and Truesdell, A.H., 1973: An empirical Na-K-Ca geothermometer for natural waters. *Geochim. Cosmochim. Acta*, *37*, 1255-1275.

Georgsson, L.S., 1987: Application of resistivity sounding in the exploration of high-temperature geothermal areas in Iceland with examples from the Trölladyngja-Krýsuvík area, SW-Iceland. *Technical Programme and Abstracts of Exploration ´87, Toronto*, 52.

Gherardi, F., Panichi, C., Caliro, S., Magro, G., Pennisi, M., 2000: Water and gas geochemistry of the Euganean and Berician thermal district (Italy). *Applied Geochemistry, 15*, 455-474.

Giggenbach W. F., 1987: Redox processes governing the chemistry of fumarolic gas discharges from White Island, New Zealand, Applied Chemistry, 2, 143-161.

Giggenbach, W.F., 1988: Geothermal solute equilibria. Derivation of Na–K–Mg-Ca geoindicators. *Geochim. Cosmochim. Acta,* 52, 2749–2765.

Giggenbach, W.F., 1991: Chemical techniques in geothermal exploration. In: D'Amore, F. (coordinator), *Application of geochemistry in geothermal reservoir development*. UNITAR/UNDP publication, Rome, 119-142.

Giggenbach, W.F., and Goguel, R.L., 1989: *Collection and analysis of geothermal and volcanic water and gas discharges*. Department of Scientific and Industrial Research, New Zealand, report CD2401, 81 pp.

Giggenbach, W.F., Gonfiantini, R., Jangi, B.L., and Truesdell, A.H., 1983: Isotopic and chemical composition of Parbati Valley geothermal discharges, NW Himalaya, India. *Geothermics, 12*, 199-222.

Giggenbach, W.F., Sheppard, D.S., Robinson, B.W., Stewart, M.K., and Lyon, G.M., 1994: Geochemical structure and position of the Waiotapu geothermal field, New Zealand. *Geothermics, 23*, 599-644.

Goff, F., and Janik, C.J., 2000: Geothermal Systems. In: Sigurdsson, H., Houghton, B., McNutt, S., Rymer, H., Stix, J. (eds.), *Encyclopedia of Volcanoes*. Academic Press, San Diego, CA, 817–834 pp.

Gunnarsson, I., and Arnórsson, S., 2000: Amorphous silica solubility and the thermodynamic properties H_4SiO_4 in the range of 0°-350°C at P_{sat}. *Geochim. Cosmochim. Acta,* 64, 2295-2307

Ha Ngoc Hung, 1997: The use of Schlumberger sounding in geothermal exploration with an example from the Krýsuvík area, SW-Iceland. Report 7 in: *Geothermal Training in Iceland 1997.* UNU-GTP, Iceland, 137-172.

Heaton, T.H.E., and Vogel, J.C., 1981: "Excess air" in groundwater, *J. Hydrology, 50*, 201-216.
Jakobsson, S.P., 1979: Outline of the petrology of Iceland. *Jökull, 29*, 57-80.

Jónsson, J., 1978: *A geological map of the Reykjanes Peninsula*. Orkustofnun, Reykjavík, report OS/JHD 7831 (in Icelandic), 333 pp and maps.

Kebede Y., 2001: Application of the resistivity method in the Krýsuvík Geothermal area, Reykjanes Peninsula, SW-Iceland. Report 13 in: *Geothermal Training in Iceland 2001*. UNU-GTP, Iceland, 115-142.

Klein, F.W., Einarsson, P., and Wyss, M., 1973: The Reykjanes Peninsula, Iceland, earthquake swarm of September 1972 and its tectonic significance. *J. Geophys. Res., 82*, 865-888.

Larsson, D., Grönvold, K., Óskarsson, N., and Gunnlaugsson, E., 2002: Hydrothermal alteration of plagioclase and growth of secondary feldspar in the Hengill volcanic centre, SW Iceland. *J. Volcanol. Geotherm. Res.*, *114*, 275-290.

Lowenstern, J.B., Janik, C.J., Fournier, R.O., Tesfai, T., Duffield, W.I., Clynne, M.A., Smith, J.G., Weldegiorgis, L., Weldemariam, K., Kahsai, G., 1999: A geochemical reconnaissance of the Alid volcanic centre and geothermal system, Danakil depression, Eritrea. *Geothermics, 28,* 161-187.

Mariner, R.H., Evans, W.C., Presser T.S., and White, L.D**.,** 2003: Excess nitrogen in selected thermal and mineral springs of the Cascade Range in northern California, Oregon, and Washington: sedimentary or volcanic in origin? *J. Volcanol. Geotherm. Res., 121*, 99-114.

Marini, A., 1938: Il volcano Alid nella colonia Eritrea (in Italian). *L'Universo, 19*, 51-65, 131-170.

Minissale, A., Chandrasekharam, D., Vaselli, O., Magro, G., Tassi, F., Pansini, G. L., and Bhramhabut A., 2003: Geochemistry, geothermics and relationship to active tectonics of Gujarat and Rajasthan thermal discharges, India. *J. Volcanol. Geotherm. Res., 127,* 19-32.

Mohr P., Girnius A., and Rolff, J., 1978: Present-day strain rates at the northern end of the Ethiopian Rift Valley. *Tectonophysics, 44*, 141-160.

Morey, G.W., Fournier, R.O. and Rowe, J.J., 1962: The solubility of quartz in water in the temperature interval from 29 to 300°C. *Geochim. Cosmochim. Acta 26***,** 1029-1043.

Nehring, N.L., and D´Amore, F., 1984: Gas chemistry and thermometry of the Cerro Prieto, Mexico, geothermal field. *Geothermics, 13*, 75-89.

Nieva, D. and Nieva, R., 1987: Developments in geothermal energy in Mexico, part 12-A cationic composition geothermometer for prospection of geothermal resources. *Heat Recovery and CHP, 7,* 541-544.

Noda, T., and Shimada K., 1993: Water mixing model calculation for evaluation of deep geothermal water. *Geothermics, 22*, 165-180.

Ólafsson, M., 1991: *Geothermal activity in Krýsuvík. Sampling from fumaroles in autumn 1990* (in Icelandic). Orkustofnun, Reykjavík, report MO-91/06, 4 pp.

Pang, Z.H., and Reed, M., 1998: Theoretical chemical thermometry on geothermal water: problems and methods. *Geochim. Cosmochim. Acta, 62*, 1083-1091.

Pope, L.A., Hajash, A., and Popp, R.K., 1987: An experimental investigation of the quartz, Na-K, Na-K-Ca geothermometers and the effect of fluid composition. *J. Volcanol. Geotherm. Res., 31*, 151-161.

Reed M.H., 1982: Calculation of multicomponent chemical equilibria and reaction processes in systems involving minerals, gases, and an aqueous phase. *Geochim. Cosmochim. Acta, 46*, 513-528.

Reed M.H. and Spycher, N.F., 1984: Calculation of pH and mineral equilibria in hydrothermal waters with application to geothermometry and studies of boiling and dilution. *Geochim. Cosmochim. Acta*, *48*, 1479-1492.

Reed M.H., and Spycher, N.F., 2001: SOLVEQ: *A computer program for computing aqueous mineral gas equilibria* (revised edition). Department of Geological Sciences, University of Oregon, Or.

Saemundsson, K., 1979: Outline of the geology of Iceland. *Jökull, 29*, 7-28.

Stefánsson, A., and Arnórsson, S., 2000: Feldspar saturation state in natural waters. *Geochim. Cosmochim. Acta, 64*, 2567-2584.

Taran, Yu.A., Pilipenko, V.P., and Rozhkov, A.M., 1986: Geochemistry of hydrothermal solutions and gases in the Mutnovsky geothermal system. In: Sugrobov V.M. (ed.), *Geothermal and geochemical researches of high-temperature hydroterms* (in Russian), Nauka, Moscow, 140-189.

Tole, M.P., Ármannsson, H., Pang Z., and Arnórsson, S., 1993: Fluid/mineral equilibrium calculations for geothermal fluids and chemical geothermometry. *Geothermics 22*, 17–37.

Tonani, F., 1973: Equilibria that control the hydrogen content of geothermal gases. *Bull. Volcanol., 44,* 547-564.

Tonani, F. 1980: Some remarks on the application of geothermal techniques in geothermal exploration. In: *Proceedings, Adv. Eur. Geoth. Res., 2nd Symp., Strassbourg,* 428-443.

Truesdell, A.H., 1976: Summary of section III - geochemical techniques in exploration. *Proceedings of the 2nd U.N. Symposium on the Development and Use of Geothermal Resources, San Francisco, 1,* liii-lxxix.

Truesdell, A.H., 1991: Effects of physical processes on geothermal fluids, In: D´Amore, F., (coordinator), *Application of Geochemistry in geothermal reservoir development.* UNITAR-UNDP Publication, Rome, 71-92.

Truesdell, A.H., and Fournier, R.O., 1976: Calculations of deep temperatures in geothermal systems from the chemistry of boiling spring waters of mixed origin. *Proceedings of 2nd U.N. Symposium on the Development and Use of Geothermal Resources, San Francisco, 1,* 837-844.

Truesdell, A.H., and Nehring, 1978: Gases and water isotopes in a geochemical section across the Lardarello, Italy, geothermal field. *Pageoph., 117*, 276-289.

UNDP, 1973: *Investigations of the geothermal resources for power development*. United Nations Development Programme, report for the Ethiopian Government, 275 pp.

Vargas M., J.R., 1992: *Geology and geothermal consideration of Krýsuvík valley, Reykjanes, Iceland*. UNU-GTP, Iceland, report 13, 35 pp.

Verma, M.P., 2000: Chemical thermodynamics of silica: a critique on its geothermometer, *Geothermics 29*, 323-346.

Verma, S.P., and Santayo, E., 1997: New improved equations for Na/K, Na/Li and SiO_2 geothermometers by outlier detection and rejection. *J. Volcanol. Geotherm. Res., 79*, 9-23.

Williams F. M., Williams M. A. J., and Aumento, F., 2004: Tensional fissures and crustal extension rates in the northern part of the Main Ethiopian Rift. *J. African Earth Sciences, 38*, 183-197.